NTNU

Norwegian University of
Science and Technology

Earthquake and Monsoon Induced Slope Failure Effects on Hydropower Projects - An Analysis Along the Sunkoshi Valley, Nepal

Nabin Basnet

Hydropower Development
Submission date: June 2016
Supervisor: Krishna Kanta Panthi, IGB
Co-supervisor: Reginald Hermanns, IGB

Norwegian University of Science and Technology
Department of Geology and Mineral Resources Engineering

Nabin Basnet

Earthquake and Monsoon Induced Slope Failure Effects on Hydropower Projects - An Analysis Along the Sunkoshi Valley, Nepal

Trondheim, June 2016

MASTER'S THESIS: TGB4910

Main supervisor: Associate Professor Dr. Krishna Kanta Panthi

Co-supervisor: Adjunct Professor Dr. Reginald Hermanns

Department of Geology and Mineral Resources Engineering

Norwegian University of Science and Technology (NTNU)

NTNU – Trondheim
Norwegian University of
Science and Technology

NTNU
Norwegian University of Science and Technology

Department of Geology and Mineral Resources Engineering

Your ref.: MS/I11T35/IGB/NBKKP

Date: 14.01.2016

TGB4910 Rock Engineering - MSc thesis

for

Nabin Basnet

EARTHQUAKE AND MONSOON INDUCED SLOPE FAILURE EFFECTS ON HYDROPOWER PROJECTS – AN ANALYSIS ALONG THE SUNKOSHI VALLEY, NEPAL

Background

The candidate has carried out field visit during the summer 2015 to document the landslides along the Sunkoshi Valley caused by 7.8 Magnitude earthquake of 25th April 2015 and many large magnitude aftershocks. The candidate also carried bout field assessment on the Jure slide that took place during monsoon 2014, collected rock sample, data and information of damages on hydropower structures caused by both earthquake and monsoon induced landslides.

The MSc-thesis work is therefore to study on the on the earthquake and monsoon induced slope failure effect on the hydropower structure of Sunkoshi Valley that shall include following task:

- Literature review of the large magnitude earthquakes in the Himalaya and surrounding areas and discuss earthquake induced large slope failure as an example.
- Literature review on the slope failure mechanism, effect of earthquake and groundwater in the slope failure process and approaches used for slope stability assessment.
- Document and investigate landslides along Sunkoshi valley using Google Earth and other historical sources.
- Document the damage on hydropower structure caused by earthquake and monsoon induced landslide and discuss.
- Carry out stability assessment of the Jure Rock slide using kinematic, analytical and numerical approaches.
- Discuss the findings and conclude the work.

Relevant computer software packages

Candidate shall use Arc-GIS, *roc-science package* and other relevant computer software.

Background information for the study

- Relevant information about the project such as reports, maps, information and data collected by the candidate.
- The information provided by the professor about rock engineering and hydropower.
- Scientific papers, reports and books related to the Himalayan geology and slope stability.
- Scientific papers and books related to international slope failure cases.

Dr. Reginald Hermanns, Adjunct Professor at the IGB-NTNU and Team Leader of the landslides team at the Geological Survey of Norway, will act as co-supervisor of this MSc thesis.

The project work is to start on January 15, 2016 and to be completed by June 10, 2016.

The Norwegian University of Science and Technology (NTNU)
Department of Geology and Mineral Resources Engineering

January 14, 2016

Dr. Krishna K. Panthi
Associate Professor of Geological Engineering, main supervisor

Abstract

Due to various reasons like fragile geology, steep topography, highly varying climate and rainfall, many slope failures of varying sizes are very common in Nepal. Every year a lot of those events occur which cause a huge loss of life and property. Jure rockslide, which took place on 2^{nd} of August 2014, is one of the most devastating disasters related to slope instability in the recent years in Nepal. Therefore, it is chosen as the representative case to carry out slope stability assessment. During the evaluation, kinematic, limit equilibrium, as well as numerical modeling are conducted. From the analyses, it has been confirmed that the slope failure in the Jure rockslide is caused by the combination of the main discontinuity set and raised groundwater level due to rainfall.

Moreover, Gorkha earthquake (M = 7.9) hit Central Nepal on 25^{th} of April 2015 which is the largest earthquake to strike Nepal after the 1934 Nepal-Bihar earthquake. Apart from the loss of lives, the major infrastructures suffered heavy damages. So, the Sunkoshi Valley, being one of the hardest hit areas, is chosen to document the damages in hydropower projects due to the earthquake. From the documentation of damages, it has been observed that the most damages were caused due to the quake-induced rock and debris fall or shallow landslides rather than the shaking itself.

Hence, from both case studies, the slope failure processes induced by monsoon and earthquake are analysed and their effects on the hydropower projects are studied. Also, it is concluded that the earthquake and monsoon-induced slope failures greatly influence the efficient functioning of a hydropower project.

Preface

This master's thesis entitled *"Earthquake and Monsoon Induced Slope Failure Effects on Hydropower Projects - An Analysis along the Sunkoshi Valley, Nepal"* is submitted to the Department of Geology and Mineral Resources Engineering in partial fulfillment of the requirements for the degree of Master of Science in Hydropower Development.

This thesis is the final outcome of the work carried out in spring semester 2016 although the relevant data were collected during the field work in summer 2015. Associate Professor Dr. Krishna Kanta Panthi supervised this work while Adjunct Professor Dr. Reginald Hermanns was my co-supervisor.

I hereby declare that the work presented in this thesis is my own and all outside contributions have been duly acknowledged.

.....

Nabin Basnet

Trondheim, Norway

2016-06-10

Acknowledgment

At the start, I would like to express my sincere gratitude to my supervisor Associate Professor Dr. Krishna Kanta Panthi for his valuable suggestions and guidance from the start till the end of this study. Also, I am indebted to my co-supervisor Dr. Reginald Hermanns for his timely input to shape this report to this final form.

Also, I would like to thank Chhatra Bahadur Basnet, Ph.D. candidate, IGB, NTNU for his help from the beginning till the end of thesis study, more importantly during the field work in summer 2015 and laboratory testing. Also, I am grateful to Bigyan Upadhayay and Suman Thapa, Epicenter Engineering Services Pvt. Ltd., Kathmandu, Nepal for their great help and support during the data collection for this study. Furthermore, I am thankful for all the persons related to the eight hydropower projects for their cooperation in the corresponding offices as well as in the field for the collection of the relevant data.

Lastly, I am grateful to my girlfriend Saraswati for her immense love and inspiration to help me keep on moving forward at times. Also, my sincere regards to my friends and family for their direct and/or indirect contribution to the completion of this study.

N.B.

Table of Contents

Abstract i

Preface ii

Acknowledgment iii

List of Figures viii

List of Tables xi

List of Acronyms xiv

1 Introduction **1**

1.1 Background 1

1.2 Objectives and Scope of the Study 3

1.3 Methodology 4

1.4 Structure of the Thesis 5

1.5 Limitations of the Study 6

2 The Sunkoshi Valley **7**

2.1 Location and Topography 7

2.2 Climatic and Hydrological Conditions 9

2.2.1 Rainfall Characteristics 10

2.3 Geology 10

2.4 Jure Rockslide 12

3 Large-scale Natural Rock Slope Instabilities 17

3.1 Rockslide and its Development 17

3.2 Types of Rock Slope Failures 18

3.3 Causes and Controlling Factors of Rock Slope Instability 22

3.4 Effects of Earthquakes and Groundwater in Slope Failure Process 23

4 Methodologies for Stability Assessment 25

4.1 Stability Analysis 25

4.2 Stability Analysis by Conventional Methods 26

4.2.1 Kinematic Methods 27

4.2.2 Limit Equilibrium Methods (LEM) 28

4.3 Stability Assessment by Numerical Methods 31

4.3.1 Numerical Modelling of Jure Rockslide 32

5 Earthquake Impacts 37

5.1 Historical Occurrences 37

5.2 Earthquake-Induced Slope Failure 38

5.3 Case Study: Wenchuan Earthquake, China 39

5.4 The Gorkha Earthquake 40

6 Analysis of Jure Rockslide by Conventional Methods 45

6.1 Kinematic Analysis 45

6.1.1 Input for Kinematic Analysis 45

6.1.2 Analysis Results 47

6.2 Limit Equilibrium Method (LEM) 49
6.2.1 Assumptions 49
6.2.2 Back Calculation 50
6.2.3 Sensitivity Analysis 54
6.2.4 Determination of Barton-Bandis Shear Strength Parameters 55

7 Numerical Analysis of Jure Landslide 57
7.1 Input for Numerical Modeling 57
7.1.1 Laboratory Work 57
7.1.2 Discontinuity Shear Strength Parameters 59
7.2 Model Setup 61
7.3 Summary of scenarios 67
7.4 Phase^2 Results 67
7.4.1 Maximum Shear Strain 68
7.4.2 Displacement 70
7.5 Discussion of Stability Analysis Results 72

8 Earthquake Impacts on the Sunkoshi Valley 73
8.1 Salient Features of HPPs along the Sunkoshi Valley 73
8.2 Earthquake Damage Details on HPPs 74
8.2.1 Bhairabkunda HPP 74
8.2.2 Upper Bhotekoshi HPP 75
8.2.3 Upper Chaku "A" HPP 75
8.2.4 Middle Chaku HPP 76
8.2.5 Chaku Khola HPP 76

8.2.6 Lower Chaku HPP 77
8.2.7 Sunkoshi Small HPP 77
8.2.8 Sunkoshi HPP 78
8.3 Earthquake Induced Landslides in the Sunkoshi Valley 79
8.4 General Discussion on the Nature of the Damages 81
8.5 Mitigation Measures 81

9 Conclusions and Recommendations **83**
9.1 Conclusions 83
9.2 Recommendations for Further Work 84

References **85**

Appendices **92**

List of Figures

1.1 (A) Simplified geological map of the Himalaya. (B) Schematic cross section across the central Himalaya. 2

2.1 Location of Sunkoshi Valley in Nepal 7

2.2 Sunkoshi as a major contributor to Sapta Koshi River system . . . 8

2.3 Location of Jure rockslide and the hydropower projects in the Sunkoshi Valley 9

2.4 Monthly Variation of Rainfall at Barabishe from 1976 to 2005) . . . 10

2.5 Geological map of the study area 11

2.6 Jure landslide components with landslide dam 13

2.7 Tension cracks seen in Jure rockslide. 14

2.8 Rainfall data before and after the disaster recorded at Barhabise station 15

2.9 Major lineaments near the rockslide area 16

3.1 Main types of rock slope failures 18

3.2 Geometry of slope exhibiting plane failure 19

3.3 Geometric conditions for wedge failure 20

3.4 Common categories of toppling failures 21

4.1 Flowchart illustrating three levels of landslide analysis 26

4.2 Flowchart of c-ϕ back calculation method 30

5.1 (A) Map of the Himalayan arc showing historical earthquakes (B) Panel showing temporal clustering of large earthquakes along the Himalayan arc. 37

5.2 Co-seismic landslides induced by Wenchuan earthquake 39

5.3 Map showing Gorkha earthquake and its aftershocks 41

5.4 Co-seismic landslides induced by Gorkha earthquake 42

6.1 Topographic map after Jure rockslide. 46

6.2 DIPS output: Plane failure (with 20° lateral limits) 48

6.3 Slope geometries and ground water conditions for back calculation 50

6.4 Mobilized shear strength for slope failure 53

6.5 Sensitivity analysis with varying water level in tension crack 55

7.1 Topographic map of Jure site before disaster with the chosen cross-section 61

7.2 Typical recommendations for locations of artificial boundaries in slope stability analyses 62

7.3 Stress – Strain relationship 64

7.4 Final Phase² profile of Jure rockslide with SSR search area 65

7.5 Result of finite element groundwater analysis 66

7.6 Maximum shear strain results for dry cases; (UP) Analysis 1 and (DOWN) Analysis 2. 68

7.7 Maximum shear strain results for high groundwater cases; (UP) Analysis 3 and (DOWN) Analysis 4. 69
7.8 Total displacement for dry cases; (UP) Analysis 1 and (DOWN) Analysis 2. 70
7.9 Total displacement for high groundwater cases; (UP) Analysis 3 and (DOWN) Analysis 4. 71

8.1 (LEFT) Debris fall in the intake area of Bhairabkunda HPP. (RIGHT) Penstock, powerhouse, and switchyard of Bhairabkunda HPP. . . . 74
8.2 (LEFT) Penstock of Bhotekoshi HPP. (RIGHT) Scouring due to flooding after the penstock burst. 75
8.3 Cracks seen in the powerhouse of Middle Chaku HPP 76
8.4 Powerhouse of Chaku Khola HPP 77
8.5 Powerhouse of Sunkoshi Small HPP. 78
8.6 Intake of Sunkoshi HPP 79
8.7 Earthquake-induced landslides in the Sunkoshi Valley 79
8.8 Distribution of >100 m landslides in the Sunkoshi Valley 80

List of Tables

7.1 Laboratory Test Standards 58
7.2 Laboratory Test Results 58
7.3 Barton-Bandis Shear Strength Parameters 60
7.4 Boundary Setup for Phase² model 63
7.5 Boundary Setup for Finite Element Groundwater Analysis in Phase² model 66

8.1 Salient features of HPPs along Sunkoshi Valley 73

List of Acronyms

CAD	Computer Aided Drawing
CRSRF	Critical Shear Strength Reduction Factor
DEM	Digital Elevation Model
ESRI	Environmental Systems Research Institute
FDM	Finite Difference Method
FEM	Finite Element Model
FLAC	Fast Lagrangian Analysis of Continua
FOS	Factor of Safety
GIS	Geographic Information System
HPP	Hydro Power Plant
IGB	Department of Geology & Mineral Resources Engineering
ISRM	International Society for Rock Mechanics
IVM	Department of Hydraulic and Environmental Engineering
JCS	Joint-wall Compressive Strength

JRC	Joint Roughness Coefficient
LEM	Limit Equilibrium Method
MCT	Main Central Thrust
MoI	Ministry of Irrigation
MW	Megawatt
NPC	National Planning Commission
NPR	Nepalese Rupees
NSET	National Society for Earthquake Technology
NTNU	Norwegian University of Science and Technology
Ph.D.	Doctor of Philosophy
ROR	Run Off River
SINTEF	The Foundation for Scientific and Industrial Research
SSR	Shear Strength Reduction
UCS	Uniaxial Compressive Strength
USGS	United States Geological Survey
VDC	Village Development Committee

Chapter 1

Introduction

1.1 Background

Nepal, a tiny Himalayan country located in South Asia, is also geologically placed in a seismic prone area. The primary source of the earthquake in Nepal and the Himalayan Region is due to the sliding of the Indian plate underneath the Eurasian plate, resulting in contraction effect and stress concentration (Dahal et al., 2013a). Apart from the earthquake and its related hazards, it is also susceptible to water induced disasters like landslides due to its fragile geology, steep topography, and highly varying climate.

Two representative cases of the natural calamities where the fragility of the Himalayan geology was exposed were Jure rockslide and Gorkha earthquake. The Jure rockslide occurred on the 2^{nd} of August 2014 and killed 155 people (Jaboyedoff et al., 2015). Similarly, the Gorkha earthquake (M 7.8) struck on the 25^{th} of April 2015 (USGS, 2015b)) when 8686 people lost their lives and about half million houses were completely destroyed (NSET, 2015). Also, the hydropower projects along the Sunkoshi Valley suffered substantial damages from those dis-

asters. Despite the vulnerabilities mentioned above, not much has been done for the preparedness with regards to upcoming disasters.

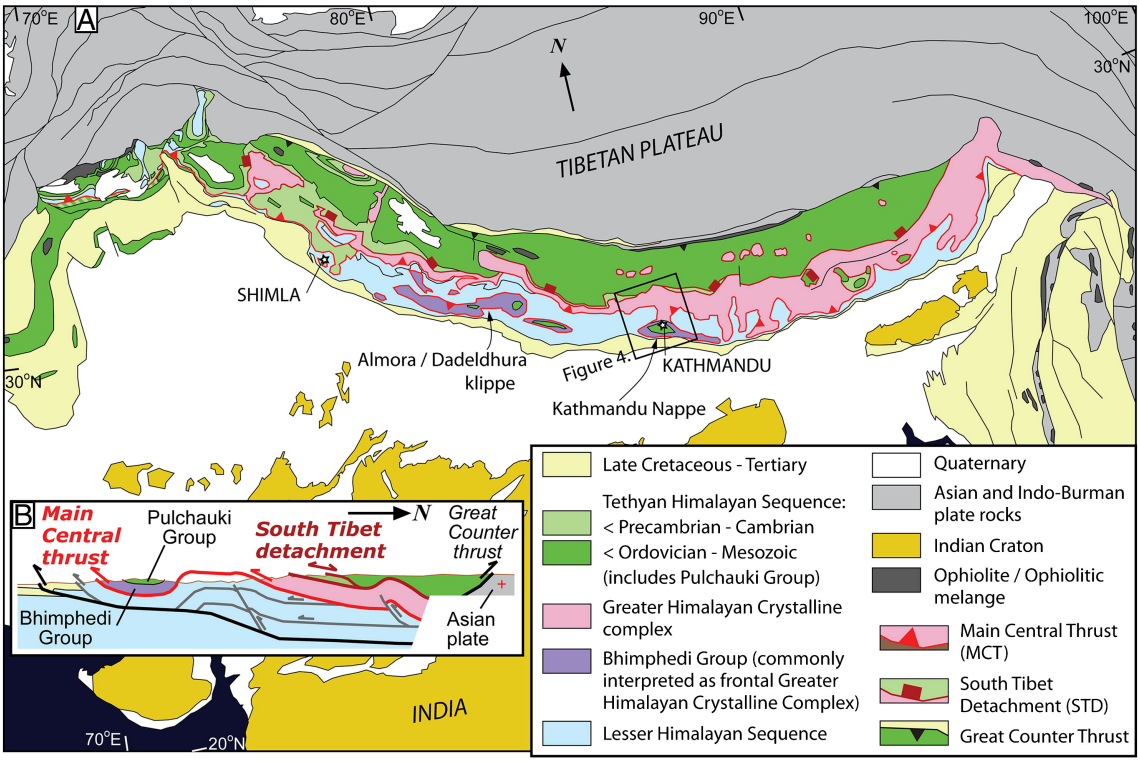

Figure 1.1: (A) Simplified geological map of the Himalaya, based on Aikman et al. (2008), DiPietro and Pogue (2004), Larson et al. (2010a), Long and McQuarrie (2010), Mitchell et al. (2007), Rao et al. (2000), Webb et al. (2007), Yin and Harrison (2000), Yin (2006), and Yin et al. (2010) as cited in (Webb et al., 2011). (B) Schematic cross section across the central Himalaya.

Currently, Nepal is facing up to 18 hours of power-cuts in the dry season due to insufficient power production. With a lot of fast flowing rivers, hydropower remains the key in fulfilling the energy deficit. With the need for some high head reservoir projects shortly, the safety of the structures and people remains a burning issue considering the fragile geology of Nepalese Himalaya. So, the slope stability is one of the important aspects of sustainable hydropower development in Nepal.

In this thesis, Jure rockslide is analyzed as a case study for investigating monsoon induced slope failure. Similarly, Gorkha earthquake will also be analyzed to see the hydropower damages in the Sunkoshi Valley.

1.2 Objectives and Scope of the Study

The main objectives of the study are:

1. Assessment of earthquake and monsoon-induced slope failure effects on hydropower projects.

2. Recommend some mitigation measures to reduce damages in the hydropower projects due to the earthquake and monsoon-induced slope failures.

3. Analysis of Jure rockslide by kinematic, limit equilibrium and numerical methods.

The scope of this study covers the following extent:

1. Document and investigate landslides along Sunkoshi Valley using Google Earth and other historical sources.

2. Document the damages on hydropower structures along Sunkoshi Valley caused by the earthquake and monsoon-induced landslides and discuss.

3. Carry out stability assessment of the Jure rockslide using kinematic, LEM and numerical approaches.

1.3 Methodology

The following methodology has been applied to the study:

1. **Literature Review**

   Literature review has been done to receive the background information on

   - Large-magnitude earthquakes in the Himalaya and the surrounding areas.
   - Slope failure mechanism and approaches used for slope stability assessment.
   - Effect of earthquake and monsoon in the slope failure processes.

2. **Data Collection**

   Relevant data were acquired from Nepal during the field work in summer 2015. A rock sample collected from the Jure rockslide deposit was transported to the laboratory at Department of Geology and Mineral Resources Engineering, NTNU for testing. Required data were acquired from different sources, and relevant photographs were taken for further assessment.

3. **Laboratory Work**

   Laboratory work was carried out at various times between January and May 2016. The UCS value, Young's Modulus, basic friction angle, sonic velocity, mineralogical composition of the rock sample among others was found out from the testing.

4. **Analysis**

   Slope Stability Analysis of Jure rockslide was carried out which consist of

three steps. At first, kinematic analysis has been carried out, followed by back calculation using Limit Equilibrium Method. Lastly, numerical modeling is done using the input parameters from both the back calculation and the laboratory testing results.

5. **Assessment**

   The damages in the hydropower projects in the Sunkoshi Valley have been assessed based on field observations and photographs.

1.4 Structure of the Thesis

There are nine chapters altogether in this thesis. The rest of the thesis is structured as follows:

- Chapter 2 gives general information about the Sunkoshi Valley and the Jure rockslide.

- Chapter 3 includes the literature review of large-scale natural rock slope instabilities, their types and the effects of earthquake and groundwater on them.

- Chapter 4 includes the literature review of the methodologies which can be adopted for stability assessment. Moreover, some of the relevant conventional and numerical methods are discussed in details.

- Chapter 5 gives general information about the Gorkha earthquake and also some literature review about the impacts caused by the earthquakes.

- Chapter 6 describes the analysis of Jure rockslide by conventional methods, namely kinematic and limit equilibrium techniques.
- Chapter 7 shows the numerical analysis of the Jure rockslide and discusses about the results.
- Chapter 8 documents the incurred earthquake damages on hydropower projects and earthquake-induced landslides along the Sunkoshi Valley.
- Chapter 9 outlines the conclusions drawn from the study and also recommends some further works.

1.5 Limitations of the Study

One of the major problems faced during the study was the estimation of input parameters for modeling. Whenever required, some of the relevant parameters were chosen from the literature to reflect the real situation in the field as close as possible.

Also, the analysis of the Jure rockslide was limited to the upper portion only due to time constraints. Furthermore, a simplified model has been chosen for the analysis although the actual rockslide might be far more complex than assumed.

Lastly, since the slope was still active with frequent debris falls, geological mapping on the slope face was not possible due to which the parameters verified by the modeling could not be compared with reliable field data.

Chapter 2

The Sunkoshi Valley

2.1 Location and Topography

Figure 2.1: Location of the study area in Nepal (Basemap: arcgis.com)

Geographically, the Sunkoshi Valley stretches from Nepal-China border to Tribeni (refer figure 2.2). But, the study area for this thesis is just the part of the Sunkoshi Valley extending from Dolalghat (27° 38’ 4.56" N, 85° 42’ 8.28" E, 967 m) where

Indrawati River meets Sunkoshi River up to the Nepal-China border at Tatopani (27° 58’ 48" N, 85° 55’ 48" E, 2474 m) (GoogleEarth, 2016). So, whenever the term "Sunkoshi Valley" is mentioned in this thesis, it only refers to the study area as stated above. Topographically, the area is located in the middle mountain region. The middle mountain region varies from 300 to 3000 m with a total area of 42,904 km² (Lillesø et al., 2005).

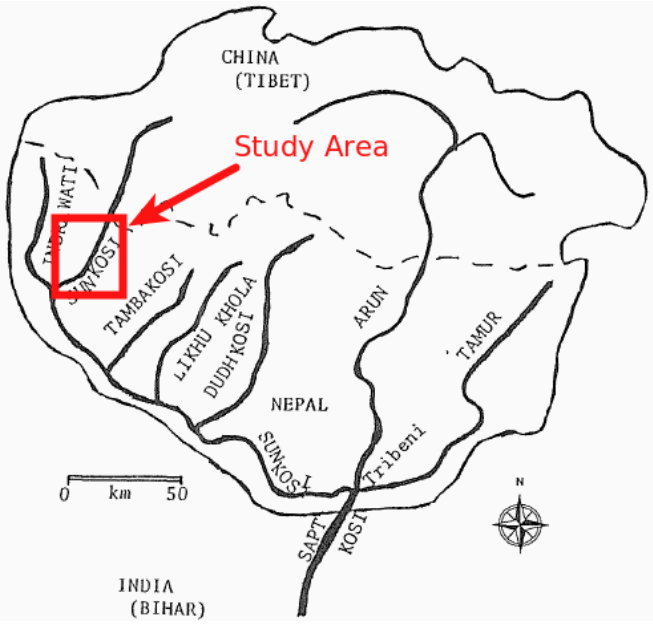

Figure 2.2: Sunkoshi as a major contributor to Sapt Koshi River system (Kattelmann, 1991).

For this study, a rockslide site and eight different hydropower projects (HPPs) which are located in the Sunkoshi Valley are chosen as shown in figure 2.3. The Araniko highway follows the study area all the way from Dolalghat up to the Nepal-China border. All the hydropower projects are located in the main corridor except Upper Chaku "A", Middle Chaku and Chaku Khola, which lie in the Chaku river corridor.

Figure 2.3: Location of Jure rockslide and the hydropower projects in the Sunkoshi Valley.

2.2 Climatic and Hydrological Conditions

The climate in the Sunkoshi Valley is subtropical which is the most common climate of the middle hills located above river valleys (Lillesø et al., 2005).

Hydrologically, the Sunkoshi River (comprising of five rivers namely Indrawati, Sunkoshi, Tamakoshi, Likhu Khola and Dushkoshi) is one of the three major tributaries of Saptakoshi river system as shown in figure 2.2. In the study area, the main river running through the valley starting from Nepal-China border is Bhotekoshi river which is named Sunkoshi after being mixed with Sunkoshi river near Sunkoshi Bazaar.

2.2.1 Rainfall Characteristics

Rainfall data collected between 1976 to 2005 in Barhabise gauging station which is located in the Sunkoshi Valley (about six km NE from Jure rockslide) shows that it receives almost 3,000 mm of annual rainfall with the monsoon season accounting for more than 80% of the total. The average monthly variation of rainfall is shown in figure 2.4. Also, the highest 24-hour rainfall recorded at this station is 166 mm dated 29th of July 1982. These data indicate that the area falls in a very high precipitation zone, and there is a probability of intense rainfall events in short durations as well (Pokharel et al., 2014).

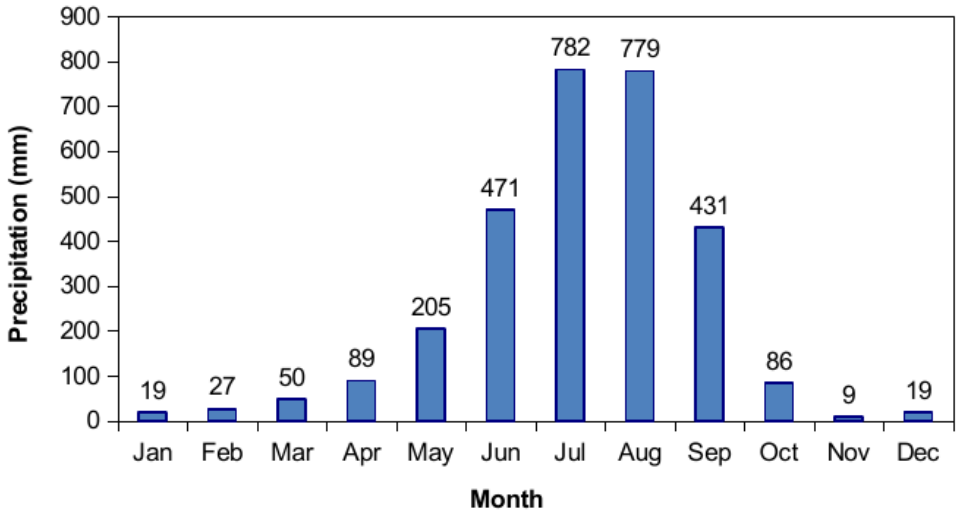

Figure 2.4: Monthly Variation of Rainfall at Barabishe from 1976 to 2005 (Pokharel et al., 2014).

2.3 Geology

Geologically, this area is underlain by Kuncha formation which is the oldest rock in the Lesser Himalaya (Champati Ray and Chattoraj, 2014). The most common characteristics of the Kuncha formation are well-developed lineation and orien-

tation towards northeast–southwest (Dhital, 2015).

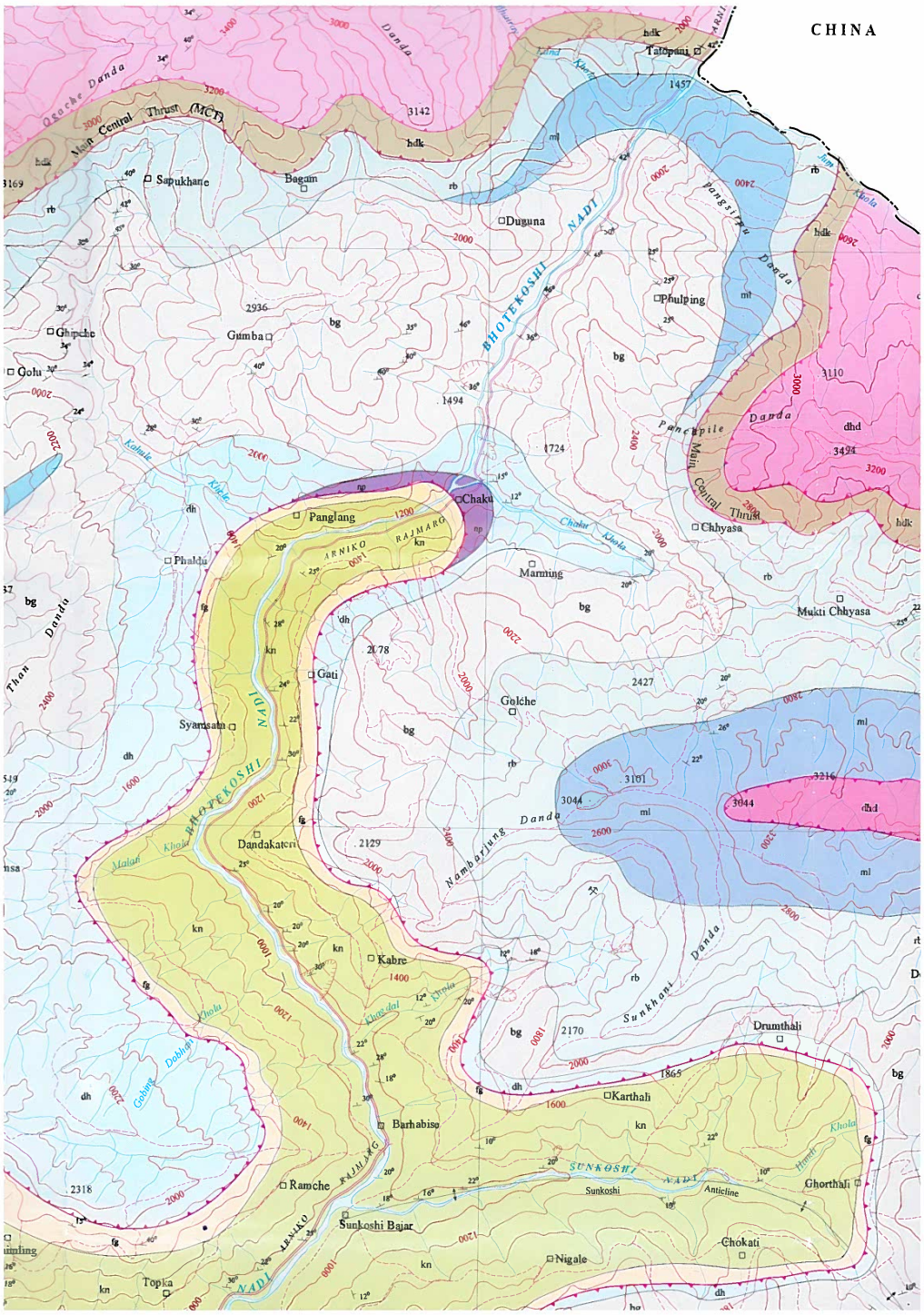

Figure 2.5: Geological map of the study area. The light green color in the map indicates kuncha formation. (Source: Department of Mines and Geology, Ministry of Industry, Nepal)

Referring the geological map in figure 2.5, the main rock types found in the study area are phyllite, limestone, slate, dolomite, quartzite, amphibolite and gneiss of the Pre-Cambrian era. Moreover, the rocks are clearly anisotropic, strongly folded, foliated and jointed due to the intense deformation as a result of thrusting and faulting (Panthi, 2006). The Main Central Thrust (MCT) crosses the Sunkoshi Valley near the Nepal-China border at Tatopani while a local thrust zone is also seen passing EW near Chaku (shown inside the purple area in figure 2.5).

2.4 Jure Rockslide

On 2^{nd} of August 2014 at 2.36 AM, a huge rockslide blocked the Sunkoshi River upstream of Jure village (70 km Northeast of Kathmandu, Nepal) in the border of Mankha and Ramche Village Development Committee (VDC). This disaster killed about 155 people, wrecking 120 houses completely and 37 partially (Jaboyedoff et al., 2015). Due to the rockslide, the Araniko Highway, which serves as the main connection to China, was washed off. Apart from that, the powerhouse of Sunkoshi Small HPP was completely submerged due to the formation of the dammed lake and the transmission lines of the upstream HPPs were damaged as well.

The Jure rockslide dammed the river, creating a 2 km long lake as seen in figure 2.6. It took 45 days for the authorities and the army to drain the lake to prevent a potential dam failure and a disaster by flooding downstream side. Also, a temporary road was built very quickly in the opposite slope of the rockslide. After the dam was breached, the intake of Sunkoshi hydropower plant located about 1

km downstream suffered some damages due to the abrupt increase in discharge. The Araniko Highway was reopened in November 2014 crossing the rockslide deposit to reach Nepal-China border at Tatopani (Jaboyedoff et al., 2015).

Figure 2.6: Jure landslide components with landslide dam. The red line is the resistant layer dividing the upper and the lower part. The intake of Sunkoshi Hydropower Project is shown in the yellow circle (Modified from KathmanduPost (2014))

.

Before the disaster, some movements were seen in the slope face as early as 2012 as seen from GoogleEarth (2016) historical imagery archives as shown in figure 2.7. It shows the possible tension cracks and also outlines the final boundaries of the rockslide. The report published by MoI (2014) also confirms the presence of the tension cracks in the crown part of the rockslide during the field visits after the disaster.

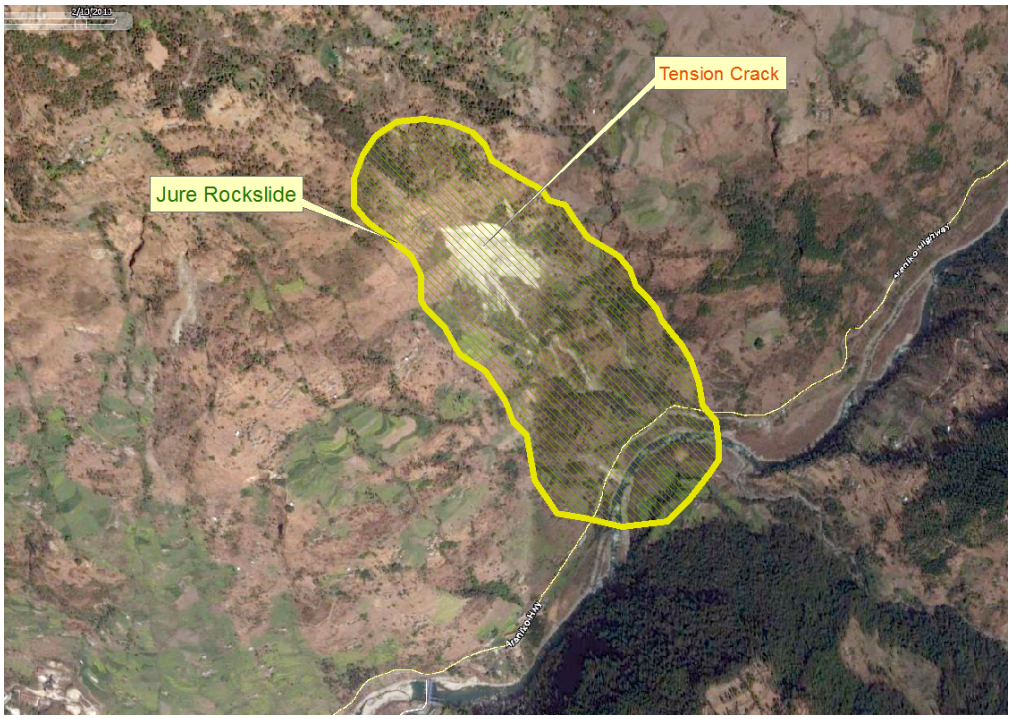

Figure 2.7: Tension cracks seen in Jure rockslide as of 13^{th} of February 2013. Modified from GoogleEarth (2016) historical archives.

As seen from figure 2.4, July-August is the peak monsoon period in the area. The daily rainfall data as recorded from the Barhabise Meteorological Station of Department of Hydrology and Meteorology, Ministry of Population & Environment, Nepal is shown in figure 2.8.

As observed in figure 2.8, two of the highest rainfall records of 70.2 mm and 70.4 mm have been registered on 30^{th} and 31^{st} of July while the actual disaster occurred on the early morning of 2^{nd} of August. The heavy rainfall obviously increased the water table in the Jure slope which already had some movements earlier. The effect of the high groundwater is analysed using the limit equilibrium method in chapter 6 as well as in the numerical model of the rockslide in chapter 7.

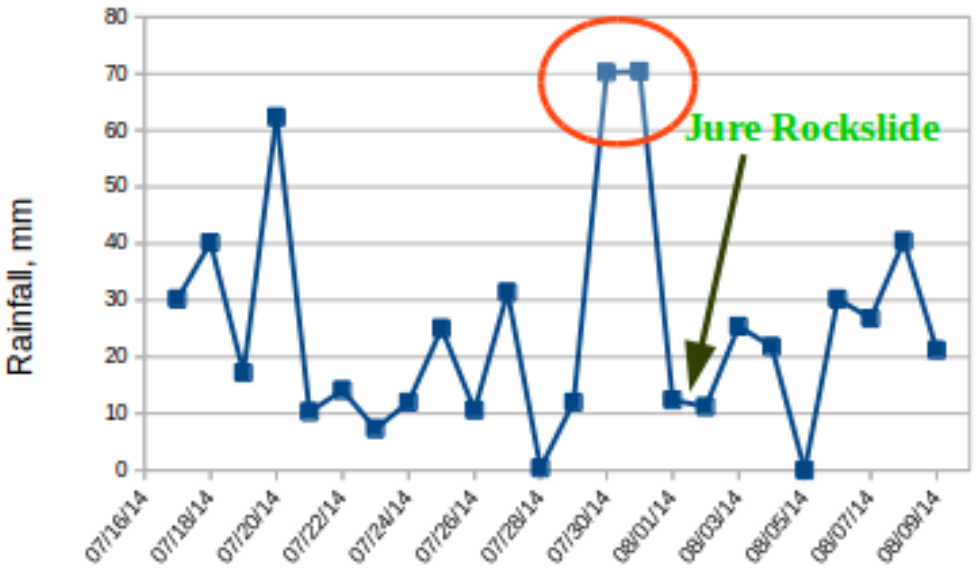

Figure 2.8: Rainfall data before and after the disaster recorded at Barhabise station. The highest rainfall records were observed just before the catastrophe. Modified from MoI (2014).

The rockslide area lies very close to Main Central Thrust zone (Refer figure 1.1) and primarily, it is traversed by two sets of noticeable joints oriented in NW-SE and NE-SW directions as shown in figure 2.9.

An NW-SE lineament (shown as a solid line in figure 2.9) passes through the landslide zone showing the overall weakness in the structure of the strata. The entire landslide mass can be divided into two distinct zones with one resistant layer in between (refer figure 2.6). On 2^{nd} of August 2014, failure occurred on both portions; where rockslide was seen in the upper portion whereas rock and debris slide was observed in the lower part (Champati Ray and Chattoraj, 2014). In this study, only the upper portion has been analysed through kinematic, LEM and numerical modeling.

Figure 2.9: Major lineaments (dashed lines) near the rockslide area. The most prominent lineament in NW-SE direction is through the landslide zone (solid line) (Champati Ray and Chattoraj, 2014).

Chapter 3

Large-scale Natural Rock Slope Instabilities

3.1 Rockslide and its Development

According to Terzaghi (1950) and Leroueil et al. (1996) as cited in Hungr et al. (2013), a landslide is a physical staged process that gradually develops in time. Based on history, the total mass movement can be termed as comprising of pre-failure deformations, the failure itself and post-failure displacements (Skempton and Hutchinson, 1969 as cited in Hungr et al. (2013)). Hungr et al. (2013) define the term "failure" as:

"Failure is the single most significant movement episode in the known or anticipated history of a landslide, which usually involves the first formation of a fully-developed rupture surfaces as a displacement or strain discontinuity."

Thus, by definition, a rockslide is a landslide that involves the mass movement of rock material (Hungr et al., 2013). When assessing a possible rockslide, it is essential to evaluate the causes of the formation of an unstable slope and also the potential triggers of failure, as they may help to predict the future behaviour and explain kinematic characteristics. Additionally, they may also help to obtain

more reliable estimates of material properties during deformation and failure. The Jure rockslide is assessed to be a planar rockslide which by definition is an extremely rapid sliding off a rock mass on a planar rupture surface with little or no internal deformation. Moreover, the sliding mass may be separating from stable rock along a deep, vertical tension crack (Hungr et al., 2013).

3.2 Types of Rock Slope Failures

Due to the difference in geological structures, the corresponding rock slope failures are also different. Figure 3.1 shows four of the idealized failure modes in rock slopes. However, in real scenarios, the failure might be a combination of more than one type of those failure modes (Wyllie and Mah, 2004).

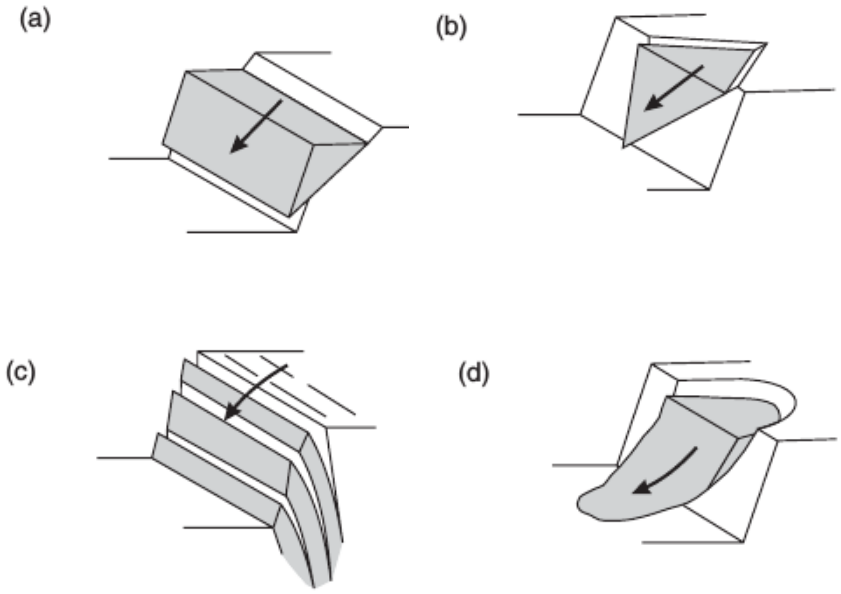

Figure 3.1: Main types of rock slope failures: (a) plane failure; (b) wedge failure; (c) toppling failure; and (d) circular failure. (Wyllie and Mah, 2004)

The first three rock slope failure types are described in more details below:

1. **Plane Failure**

   The general geometrical conditions to be fulfilled for a plane failure according to Wyllie and Mah (2004) (refer figure 3.2) are as follows:

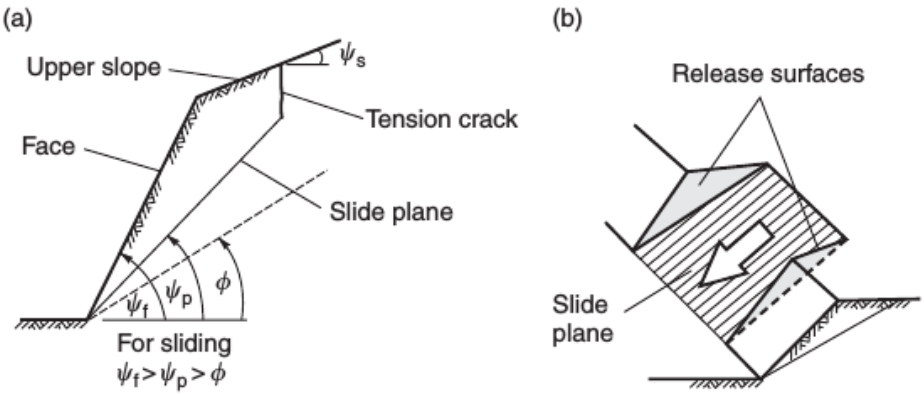

Figure 3.2: Geometry of slope exhibiting plane failure: (a) cross-section showing planes forming a plane failure and (b) release surfaces at ends of plane failure. (Wyllie and Mah, 2004)

- The plane on which sliding occurs must strike parallel or nearly parallel (within approximately ±20°) to the slope face.
- The sliding plane should "daylight" in the slope face, which means that the dip angle of the plane must be smaller than the dip angle of the slope face, that is, $\psi_p < \psi_f$ (figure 3.2(a)).
- The dip angle of the sliding plane must be larger than the angle of friction of this plane, that is, $\psi_p > \phi$ (figure 3.2(a)).
- The upper end of the sliding surface either crosses the upper slope or ends in a tension crack.
- Release surfaces must be present in the rock mass which provide negligible resistance to sliding to specify the lateral boundaries of the slide.

Alternatively, failure can occur on a sliding plane passing through the convex “nose” of a slope.

2. **Wedge Failure**

The general geometrical conditions to be fulfilled for a wedge failure according to Wyllie and Mah (2004) (refer figure 3.3) are as follows:

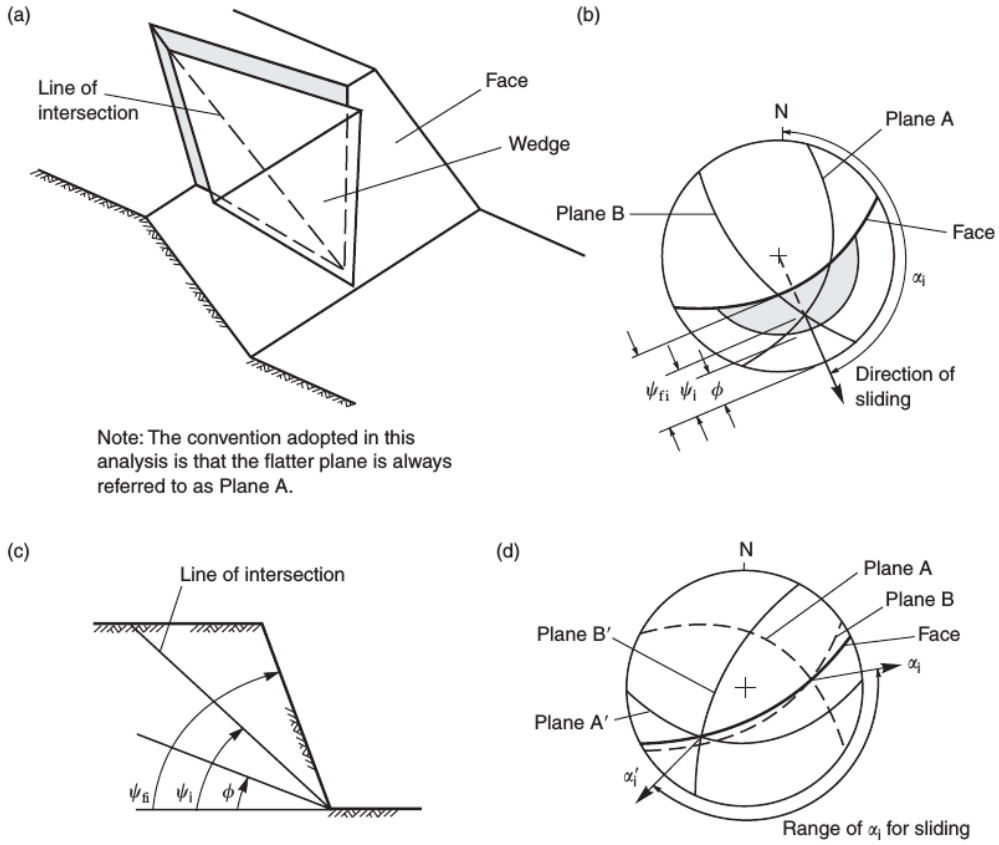

Figure 3.3: Geometric conditions for wedge failure : (a) pictorial view ; (b) stereoplot showing the orientation of the line of intersection, and the range of the plunge of the line of intersection ψ_i ; (c) view of slope at right angles to the line of intersection; (d) stereonet showing the range in the trend of the line of intersection α_i (Wyllie and Mah, 2004)

- Two planes will always intersect in a straight line (figure 3.3(a)).
- The plunge of the line of intersection must be flatter than the dip of the face, and steeper than the average friction angle of the two slide

planes, i.e. $\psi_{fi} > \psi_i > \phi$ (figure 3.3(b) and (c)).

- The line of intersection must dip in a direction out of the face for sliding to be feasible; the possible range in the trend of the line of the intersection is between ψ_i and $\psi_i^{'}$ (figure 3.3(d)).

3. **Toppling Failure**

   This failure mode involves rotation of columns or blocks of rocks about a fixed base (Wyllie and Mah, 2004). Goodman and Bray (1976) (as cited in Wyllie and Mah (2004)) have classified toppling failure into three classes; namely, block toppling, flexural toppling and block flexure toppling as shown in figure 3.4.

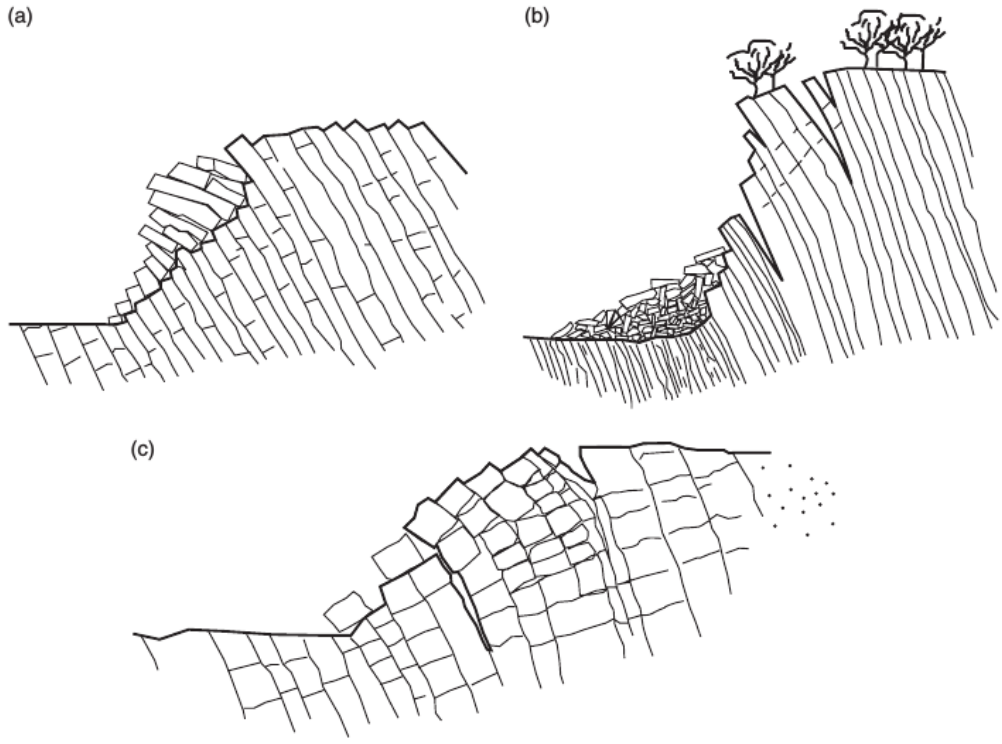

Figure 3.4: Common categories of toppling failures: (a) block toppling, (b) flexural toppling, and (c) block flexure toppling (Goodman and Bray (1976) as cited in Wyllie and Mah (2004))

3.3 Causes and Controlling Factors of Rock Slope Instability

A rock slope instability is a consequence of the high degree of rock damage which shows both spatial and temporal variation. According to Stead and Eberhardt (2013), it has characteristic damage distribution associated with variations in:

- Slope topography
- Failure surface morphology
- Failure surface geometry
- Failure mechanism
- Lithology
- Geological structure

Certain areas of a slope may be susceptible to increased damage either due to driving forces, water pressure, or in relation to the existence of pre-existing tectonic damage (Stead and Eberhardt, 2013). Moreover, as stated in Nilsen and Palmstrøm (2000), in principle, the geological and non-geological factors that govern a rock slope instability are in particular:

- Rock type boundaries and mechanical properties
- Faults and weakness zones
- Detailed jointing
- Groundwater and climatic conditions

- Rock stresses
- Geometrical conditions
- Blast vibrations and potential earthquake activity

3.4 Effects of Earthquakes and Groundwater in Slope Failure Process

Earthquake and groundwater are the most common reasons of slope instability problems. Thus, in recent years, it has received increasing attentions and become a crucial issue. However, the dynamic response and failure mode of the slope subjected to seismic forces and varying groundwater conditions simultaneously still a difficult problem. The research carried out by Huang et al. (2015) showed that the slopes behaved differently under near and far field earthquakes. Furthermore, the location of the damage were also varying in different groundwater conditions. The destruction started at the top of the slope when there was no groundwater while it started at the toe of the slope when the slope had high groundwater levels. Besides, the top of the slope showed obvious seismic subsidence phenomenon after the earthquake. Moreover, the existence of the groundwater also had a certain effect of damping (Huang et al., 2015).

Chapter 4

Methodologies for Stability Assessment

4.1 Stability Analysis

According to Nilsen and Palmstrøm (2000), the analysis of rock slope stability typically involves a three-step procedure, namely;

1. Definition of the potential stability problem.
2. Quantification of input parameters.
3. Calculation of stability.

Based upon the complexity of the failure mechanism, a landslide analysis can be divided into three different levels; namely, Kinematic & Limit Equilibrium Analysis, Continuum & Discontinuum Numerical Methods and Hybrid Finite-/Discrete Element with Fracture (Stead et al., 2006), which are illustrated and described in figure 4.1.
Depending upon the movement types, the three levels can also be classified as simple translation, complex translation and complex translation/rotation as shown.

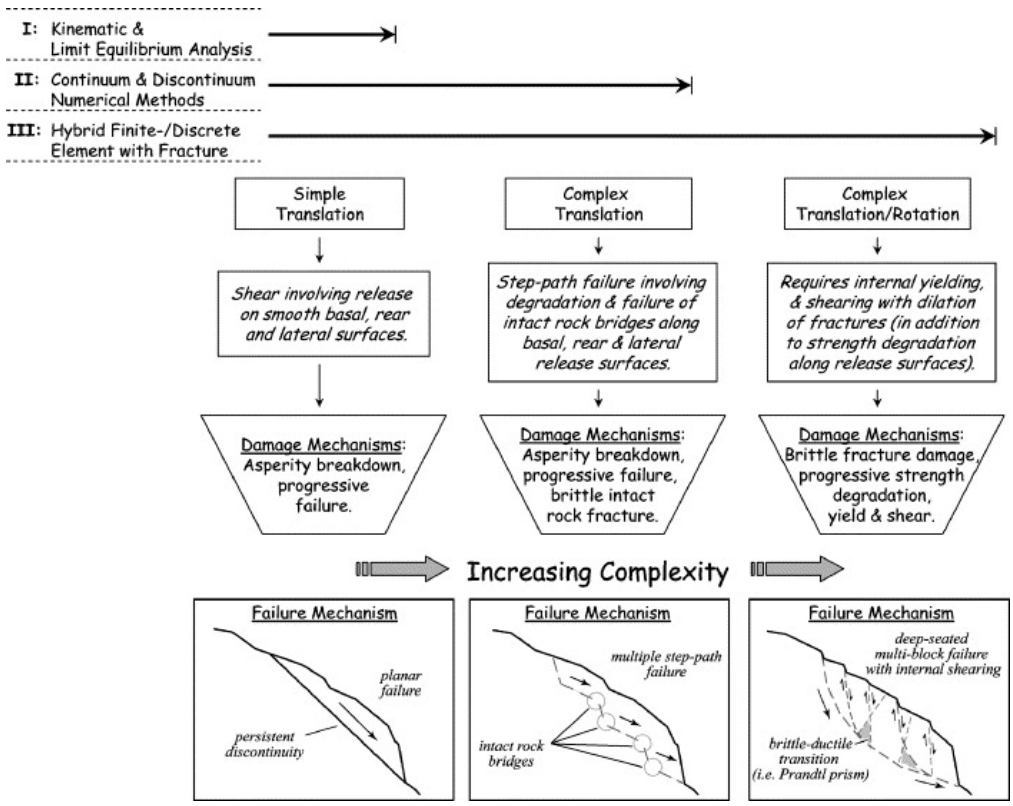

Figure 4.1: Flowchart illustrating three levels of landslide analysis and the modes of translational/rotational failure they apply to (Stead et al., 2006).

.

4.2 Stability Analysis by Conventional Methods

According to Eberhardt (2003), the conventional methods of rock slope analysis can be divided into:

- Kinematic (using stereographic interpretation)
- Limit Equilibrium (LE)
- Physical Modelling
- Rockfall Simulators

The conventional methods for slope stability analysis are principally founded on the critical stress state (or the limit equilibrium state). The critical stress state indicates the potential failure of slope occurring along the entire slip surface where a critical state is reached at the same time, therefore, the critical stress state is considered to be a peak-stress state (Lu, 2015).
The kinematic and LE techniques represent the more common conventional methods which are described in more details in the subsequent subsections.

4.2.1 Kinematic Methods

Kinematic methods focus on the occurrence of translational failures due to the creation of "daylighting" wedges or planes. Hence, these methods depend upon the detailed evaluation of representative shear strength characteristics and the geometry of discontinuity sets present which may contribute to block instability. The stability assessment may be carried out by using stereonet plots and/or sophisticated computer codes which concentrate on the formation of planes and wedges. For instance, the program DIPS (Rocscience, 2016a) can be used for the visualization and estimation of the kinematic feasibility of rock slopes through the use of friction cones, daylight and toppling envelopes. Moreover, the graphical and statistical analysis of the discontinuity properties can also be carried out by DIPS (Eberhardt, 2003).
The main objectives of the kinematic analysis are to identify the possible modes of failures, the sliding direction of the block and also depict the structural stability conditions. Before applying LE techniques and numerical modeling, a kinematic feasibility test is undertaken for the Jure rockslide within the scope of this

study and is presented in Chapter 6.1.

Software: DIPS (Rocscience)

The kinematic analysis of Jure rockslide is carried out using the software DIPS (version 6.016). DIPS, a software developed by Rocscience Inc., is designed for the interactive analysis of geological data based on orientation. It allows for clear visualization of structural data following the same techniques used in manual stereonets, judgement of the kinematic feasibility of the rock mass and statistical analysis of the discontinuity properties (Rocscience, 2016a).

4.2.2 Limit Equilibrium Methods (LEM)

Normally, limit equilibrium methods (LEM) are used in the analysis of slope stability problems where translational or rotational movements take place on distinguishable failure surfaces. Two types of analyses can be carried out in LEM. Either a factor of safety can be calculated or, a range of shear strength parameters at failure state can be found out through back-calculation. Generally in rock slope engineering, these techniques are the most usually adopted solution method, although many failures in real world involve complicated internal deformation and fracturing which bears little resemblance to the 2-D rigid block assumptions required for LEM. Nevertheless, LE analyses may be extremely applicable to simple block failures along discontinuities or heavily fractured or weathered rock slopes (i.e. behaving like a soil continuum). Hence, it is important to remember that whenever applicable, LEM should be used in concurrently with numerical modelling techniques to exploit the advantages of both

methods (Eberhardt, 2003).

LE is a time and cost efficient mathematical method and has therefore been an effective tool in slope stability analysis for years. Nevertheless, to get a satisfactory result with LE computations, at most times, the geology has to be oversimplified by assuming that the failure is translational. It also assumes that the failure process involves release on smooth basal, rear and lateral surfaces where the major active damage mechanisms are gradual failure and/or asperity breakdown (Stead et al., 2006).

A common parameter introduced in the LEM is termed as Factor of Safety (FOS) which is a non-dimensional scalar quantity and is defined as follows:

$$FOS = \frac{\text{shear strength of the material}}{\text{shear strength required for equilibrium}} \tag{4.1}$$

The FOS could be defined as the factor by which the shear strength of the material in slope has to be decreased for the slope to reach the state of failure. For any given problem, the slope is considered to be stable as soon as FOS is greater than one (Laouafa and Darve, 2002).

Back Calculation in LEM

Back calculation of a failed or a failing slope is probably the most reliable method for determining the shear strength parameters of a rock mass at failure. By using available information on the location & shape of the inferred sliding surface, unit weight of the rock, the groundwater conditions at the time of failure and any external forces like foundation loads and earthquake motion, if applicable, this process involves carrying out a stability analysis of the slope in question.

Thus, the stability analysis is used to calculate the shear strength parameters, namely cohesion and angle of internal friction, by setting the factor of safety at 1 (Wyllie and Mah, 2004).

Figure 4.2 describes the flowchart of c-ϕ back calculation method. A c-tanϕ graph is plotted from a specified factor of safety. Then, cohesion is assumed, and the angle of internal friction is calculated (Wu et al., 2005). In this study, the values of c and ϕ are calculated from the range of values at failure condition as described in details in chapter 6.2.2. The peak values of cohesion and friction angle of the sliding surface calculated with LEM are then used in the Phase² (Rocscience, 2016b) model as described in Chapter 7.

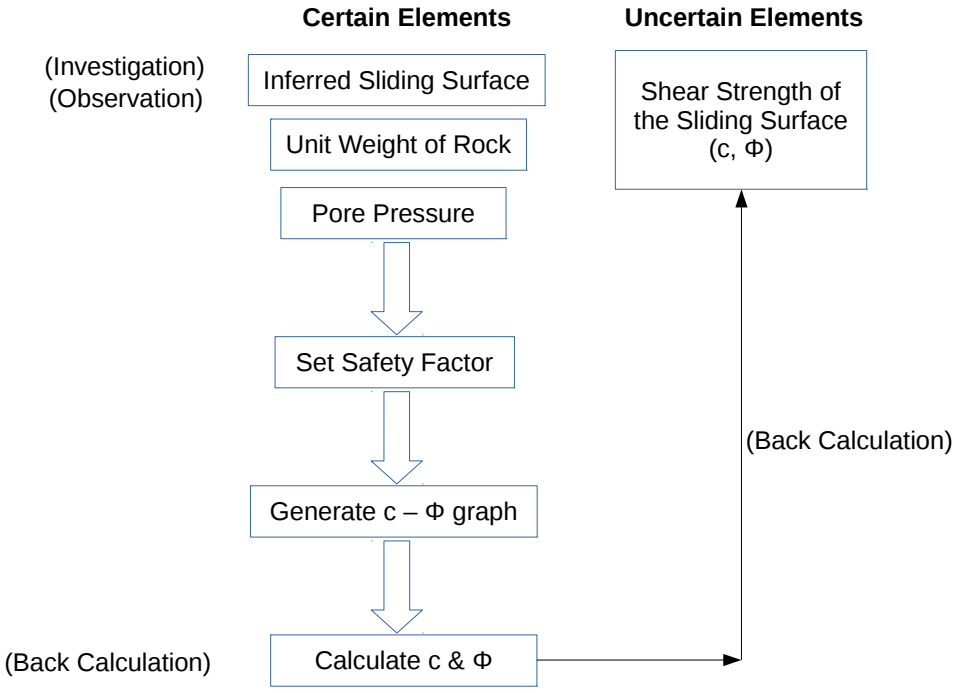

Figure 4.2: Flowchart of c-ϕ back calculation method (Modified from Shimizu, 2001 as cited in Wu et al. (2005))

4.3 Stability Assessment by Numerical Methods

Since the conventional methods of slope stability assessment are restricted to simple problems regarding their scope of application, they give little insight into slope failure mechanisms. Many rock slope stability problems in real world involve a lot of complexities considering geometry, anisotropy of material, non-linear behavior, in-situ stresses and the combination of several coupled processes (e.g. pore pressures, seismic loading and so on). So, to overcome these limitations, numerical methods have been forwarded which provide approximate solutions to the problems, which would otherwise not have been solvable using conventional techniques (e.g. LEM). The recent advances in the computing power and the accessibility of relatively affordable commercial numerical modelling codes have firmly placed the numerical simulation of potential rock slope failure mechanisms as a standard component of a rock slope investigation in many cases (Eberhardt, 2003).

Numerical modeling in rock engineering is used for analyzing rock stresses and deformation calculations. One of the major advantages of numerical modeling techniques over LEM is that the computations can be performed without assigning pre-defined failure planes which produce more reliable results. However, the accuracy of results is entirely dependent on the quality of the input parameters. Also, it is important to consider that the results are often about investigating the sensitivity of the model parameters rather than exact calculations with definite answers (Nilsen and Palmstrøm, 2000).

Numerical methods used for rock slope stability analysis may be divided into three approaches as follows according to Eberhardt (2006).

1. **Continuum modelling**

    - Most suitable for the analysis of slopes comprising of massive, intact rock, weak rocks, and soil-like or heavily jointed rock masses.
    - Procedure involves assumptions to the elements connectivity, and continuity of displacements and stresses between elements.
    - Includes finite-difference (FDM) and finite-element methods (FEM).

2. **Discontinuum modelling**

    - Best suited for slopes controlled by discontinuity behaviour.
    - Rock mass depicted as a group of distinct interacting blocks.
    - Blocks are further divided into a deformable continuum mesh following linear or non-linear stress-strain laws.

3. **Hybrid modelling**

    - Involves the coupling of continuum and discontinuum techniques to be benefitted from their key advantages.

4.3.1 Numerical Modelling of Jure Rockslide

From the discussions with the main supervisor Panthi (2016), Phase², which is a continuous numerical Finite Element Method (FEM), was selected as the software for the stability assessment of the Jure rockslide. Also, the application of Shear Strength Reduction (SSR) method in Phase² was considered fitting within the preferred objectives of this thesis.

Finite Element Method (FEM) in general

Finite Element Method (FEM) is a continuous numerical analysis technique which is widely used in rock engineering for slope stability analysis (Hammah et al., 2007). According to Hammah et al. (2007), the primarily reasons for its popularity can be attributed to its ability to:

1. Run multiple materials in a single model (material heterogeneity)
2. Readily accommodate non-linear material responses, and
3. Model complex boundary conditions.

In a finite element model, slope failure is assumed to occur "naturally" through the zones where the shear strength of the material is not sufficient to resist the shear stresses (Griffiths and Lane, 1999). This assumption is the basis for determining factor of safety (FOS) as given in equation 4.1. By this definition, FOS can be used to assess the stability of a slope, where FS > 1 indicate stable slope conditions (Wyllie and Mah, 2004).

Software: Phase² (Rocscience)

The numerical modelling of Jure rockslide is carried out using the software Phase² (version 9.004). Phase² is a 2-D, continuous, non-linear finite element program, developed by Rocscience Inc. The program is used for finite element analysis in excavation and slopes and has a broad range of applications in engineering projects, for e.g., excavation design, slope stability, groundwater seepage and probabilistic analysis, to name a few. It provides a structured, user friendly graphical environment for data entry and visualization, and a CAD based mod-

eler which allows for point and click geometry input and easy editing (Rocscience, 2016b).

Numerous analysis techniques in Phase² can be applied to model the progressive failure of Jure rockslide. This study is mainly focussed on the finite element slope stability analysis using the Shear Strength Reduction (SSR) method along with Mohr-Coulomb strength parameters. The results for the maximum shear strain and displacement contour plots are provided as output which can be used for the visualisation and the interpretation of the stability conditions of the Jure slope. The model set up, general analysis settings and input parameters used for the FEM analysis in this study are discussed in more details in Chapter 7.

Shear Strength Reduction (SSR)

The Shear Strength Reduction (SSR) method in Phase² is fully automated and calculates a Critical Strength Reduction Factor (CSRF), which is equivalent to the Factor of Safety (FOS) as defined in equation 4.1, for the slope model based on the defined input parameter values. This method can be used with either Mohr-Coulomb or Hoek-Brown strength parameters (Rocscience, 2016b).

In SSR method, the shear strength is reduced until the slope becomes unstable, and failure is defined as the point when equilibrium cannot be maintained i.e. the finite element model does not converge to a solution. The SRF value at failure is termed as the critical SRF. In a multi-staged model, SSR will only be carried out for the last stage of the model. In the case of the necessity to restrict the stability analysis to a special area of the model, an user-defined SSR search area may also be applied (Rocscience, 2016b).

SSR Search Area

Practically, slopes may have a lot of failure modes and the one with the lowest safety factor might not be the most critical failure mode. The SSR Search Area function in Phase² allows focusing the search of the more important global failure modes filtering out the other non-relevant failure modes (Rocscience, 2016b). Since we have already ascertained the failure mode of Jure rockslide as a plane failure, assigning the SSR search area is considered effective to get better results.

Finite Element Groundwater Seepage Analysis

A finite element groundwater seepage analysis in Phase² computes pore pressures from the groundwater analysis and automatically uses in the stress analysis for further computations of effective stress (Rocscience, 2016b). Since there is no information about the pore pressure values in Jure rock slope, this analysis option was considered efficient to use. The results of the finite element groundwater analysis is used as the model to analyse the high groundwater conditions as described in details in chapter 7.

Chapter 5

Earthquake Impacts

5.1 Historical Occurrences

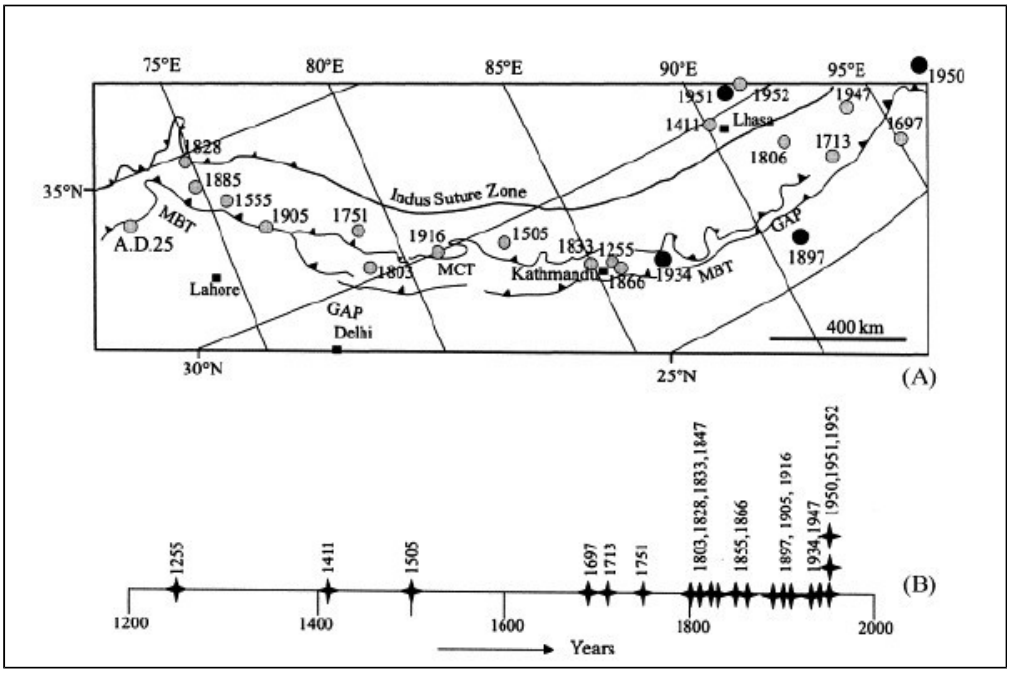

Figure 5.1: (A) Map of the Himalayan arc showing distribution of the historical earthquakes of M 7.0 and above, during the last 1000 years (solid circles denote events with M 8 and above) (B) Panel showing temporal clustering of large earthquakes along the Himalayan arc (Rajendran and Rajendran, 2005)

Earthquakes in the Himalayas have been reported as early as 1255 while major earthquakes were recorded as shown in figure 5.1 until 2000. After 2000 and before the Gorkha Earthquake, there was the Great Kashmir earthquake (M7.6) which shook Northern Pakistan and Kashmir on 8^{th} of October 2005 (Shah, 2013). The observed previous occurrences of earthquakes in the Himalayas indicate that they cannot be characterized based either on constant displacement or on constant recurrence. Sometimes, even if they are large in magnitude, they do not release all the elastic strain between the Indian and the Tibetan upper crust. This suggests that a huge earthquake can occur randomly in the Himalayas, irrespective of the time and/or place (Mugnier et al., 2013).

5.2 Earthquake-Induced Slope Failure

Earthquake-induced slope failures (or landslides) are one of the highly devastating natural disasters for the humankind. The damages from the earthquake-induced landslides is a lot worse than the actual damage related to the shaking and rupture of the earthquake itself. Although a lot of earthquake-induced landslides have occurred in Nepal before, the records of incidents are not well documented. In recent years, the advances in Geographic Information Systems (GIS) processing and remote sensing have significantly improved our ability to map earthquake-induced landslides in a more detailed and comprehensive manner (Dahal et al., 2013b).

Although the landslide movement varies to a wide range, it can be widely classified into four types: fall/topple/collapse, slide, a mixture of fall and slide and flow/spread. Through observations, the first three categories covered most of

the 70 landslides studied which occurred since 1900 and triggered by earthquakes of magnitude M>6.0 (Yamada et al., 2013).

5.3 Case Study: Wenchuan Earthquake, China

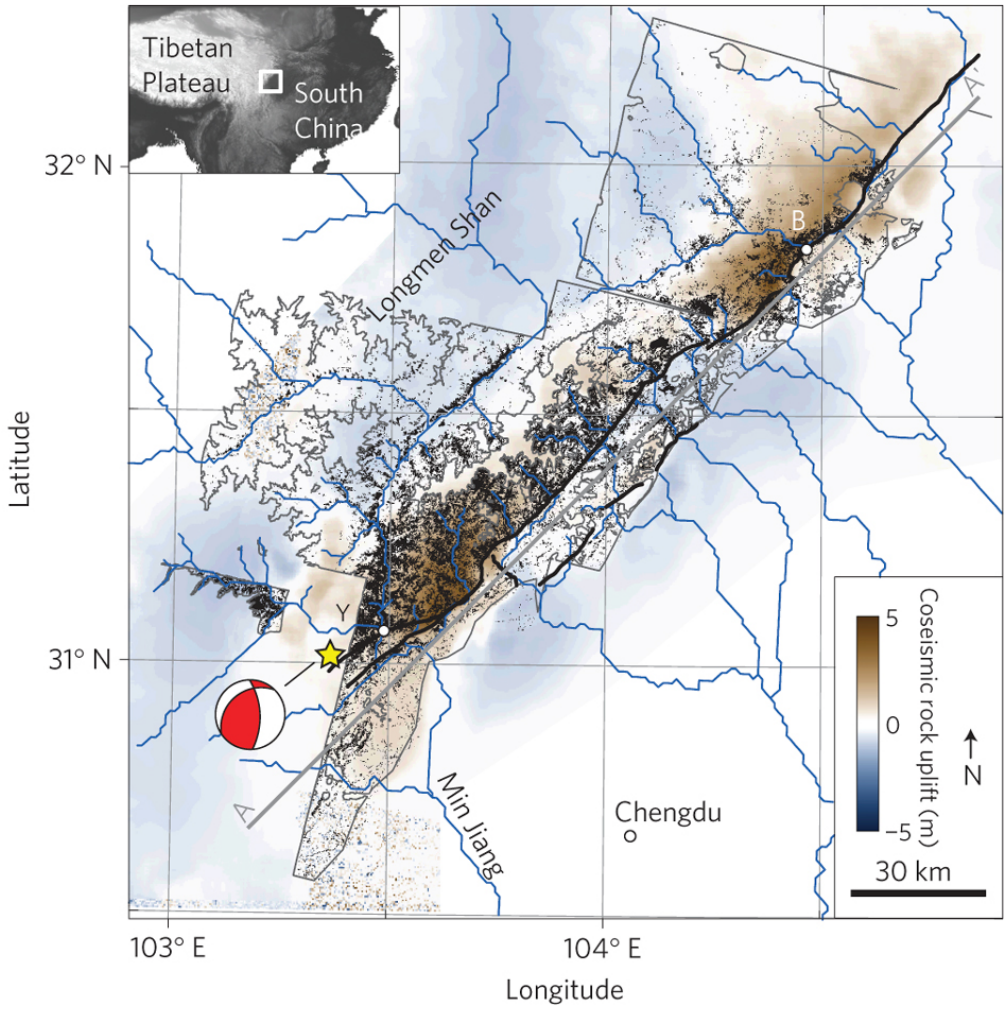

Figure 5.2: Co-seismic landslides (black polygons) induced by Wenchuan earthquake. The heavy black lines show surface rupture traces and the star denotes the epicentre. Heavy grey line shows the rupture-parallel section line onto which the results are projected. Beichuan (B); Yingxiu (Y) as cited in Parker et al. (2011)

On 12^{th} of May 2008, a massive earthquake (M 8.0) occurred in Wenchuan County in Sichuan Province, China which is also known as Wenchuan earthquake. Three

faults of the Longmenshan fracture zone located in the north-northwest part of Chengdu City moved. The slip displacement reached 8.5 m in the vertical direction. The geology of the area consists of limestone and sandstone-shale alternative layer of the Mesozoic-Paleozoic age. Numerous fall and rock avalanche type of landslides were triggered. In some cases, the velocity of the rock avalanche was even faster than 40 m/s, and more than 20,000 people were directly killed by different types of landslides (Yamada et al., 2013).

With an estimated rupture length of more than 200 km, the Wenchuan earthquake induced thousands of landslides covering an area as wide as 285×20 km. The maximum spatial density was found to be 0.3 landslide/km² and the highest density of occurrence was observed on the slopes of 30-35° (Sato and Harp, 2009).

5.4 The Gorkha Earthquake

On 25th of April 2015, an M 7.8 earthquake struck Barpak, Gorkha, 77 km NW of Kathmandu, at 11.56 local time. It is the biggest earthquake to have occurred in the Nepal Himalaya since the 1934 Nepal-Bihar earthquake. It is also the first large, modern-day event to affect the densely populated capital city of Nepal, Kathmandu (Parameswaran et al., 2015). The earthquake caused an officially estimated death toll of 8686 and also caused a massive destruction to modern-, rural- and heritage- structures in 35 out of 75 districts of Nepal (NSET, 2015).

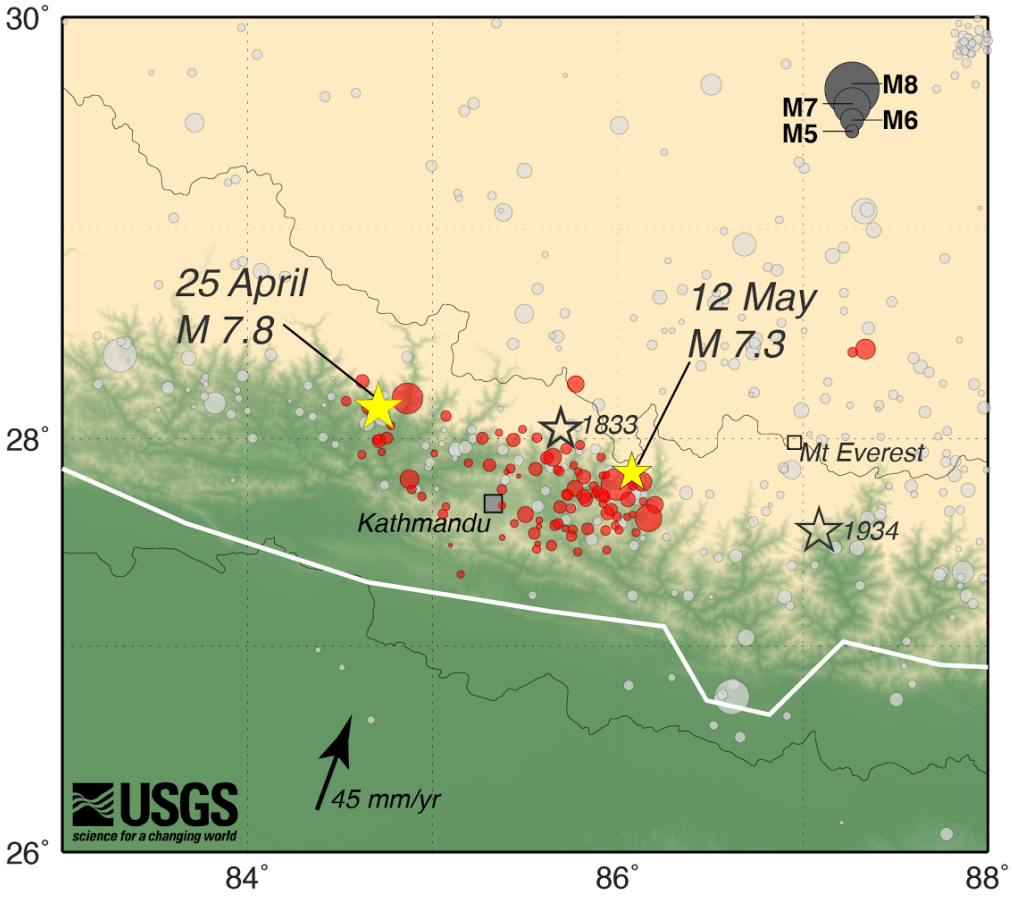

Figure 5.3: Map showing Gorkha earthquake and its aftershocks. The largest aftershock to date is M7.3. The black stars represent 1833 and 1934 earthquakes (USGS, 2015a).

The Gorkha earthquake also triggered hundreds of landslides and rock falls blocking roads and isolating villages. Avalanches on Langtang Valley, which is about 60 km NNE of Kathmandu killed several hikers and trapped much more, making this one of the deadliest tragedies in Nepal's recent history. Furthermore, as the rescue efforts were in full swing, another large earthquake occurred on 12th of May (M 7.3) with an epicenter 75 km NE of Kathmandu and about 140 km east of Gorkha as shown in figure 5.3. However, despite its larger magnitude, the Gorkha earthquake caused fewer landslides than expected. The spatial distribution of the Gorkha earthquake landslides on the downdropped block

(refer figure 5.4) shows that most of the landslides were located north of the tectonic hinge-line. Hence, the landslides were located away from the densely populated areas on the south of the hinge-line, thereby reducing the casualties (Kargel et al., 2016).

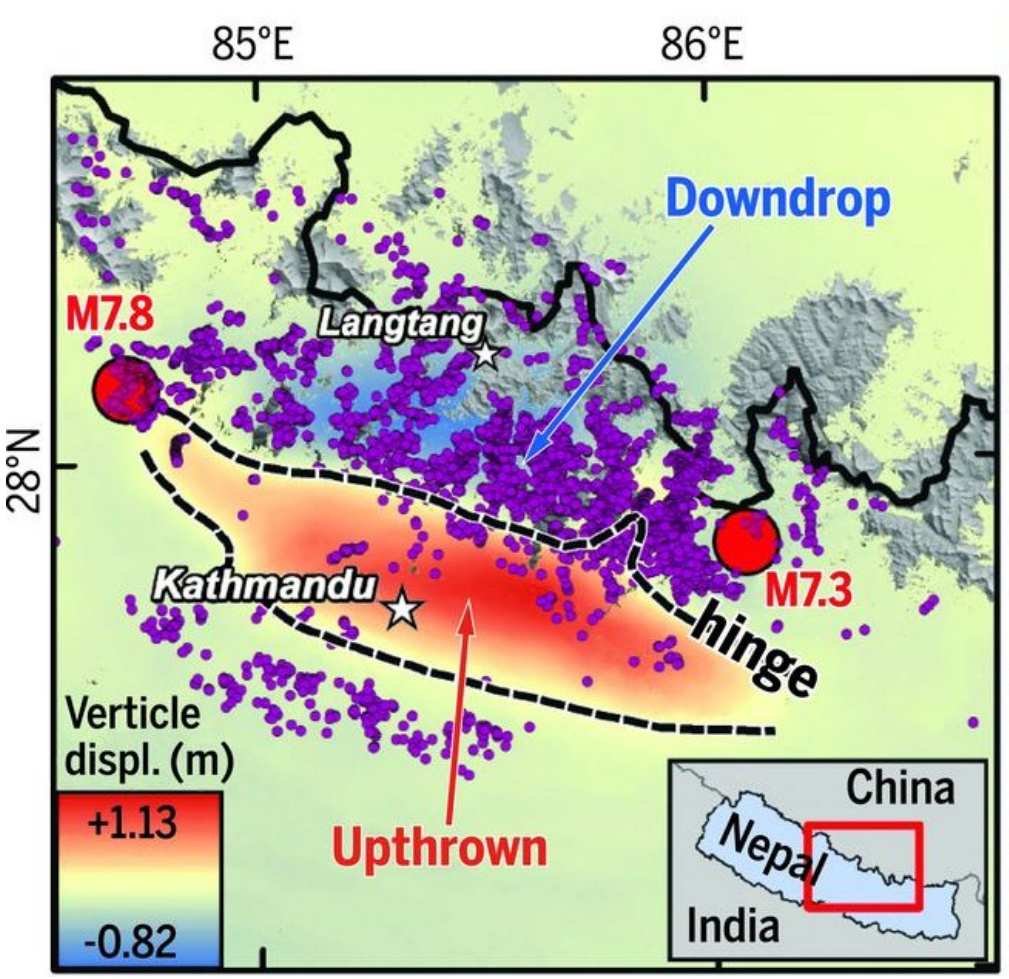

Figure 5.4: Co-seismic landslides (purple dots) induced by Gorkha earthquake. Red circles are the epicenters of the main shock and the largest aftershock. Displacements taken from the JAXA ALOS-2 ScanSAR interferogram (21 Feb and 2 May 2015 acquisitions) as cited in Kargel et al. (2016)

.

Comparing with Wenchuan earthquake as described in chapter 5.3 above, the

number of landslides triggered by it were far too small although the magnitude of both the earthquakes are similar.

Furthermore, about 115 MW hydropower generation facilities were severely damaged while 60 MW were partially damaged. Those figures are huge considering the fact that the total installed capacity (on-grid and off-grid) in Nepal is 787 MW. Also, the total damages in the electricity sector considering both generation and transmission was 21,242 NPR million (NPC, 2015).

Chapter 6

Analysis of Jure Rockslide by Conventional Methods

As described in Chapter 4.2, the conventional methods of rock slope analysis can generally be divided into kinematic and limit equilibrium techniques which are described separately in more details in the subsequent sections.

6.1 Kinematic Analysis

For the kinematic analysis, DIPS (version 6.016) has been used as already mentioned in Chapter 4.2.1.

6.1.1 Input for Kinematic Analysis

Elevation contours are generated which represent the present condition of the Jure rockslide site using spot heights from GoogleEarth (2016) with the help of ESRI (2016). The cross-sectional profile is drawn (refer figure 6.1) passing more or less through the center which is assumed to be the most active part of the rockslide. The surface of the profile is the failure plane through which the whole

slope slid downwards. So, this discontinuity set with dip/direction as 29°/136° thus calculated is used as the major input for the kinematic analysis.

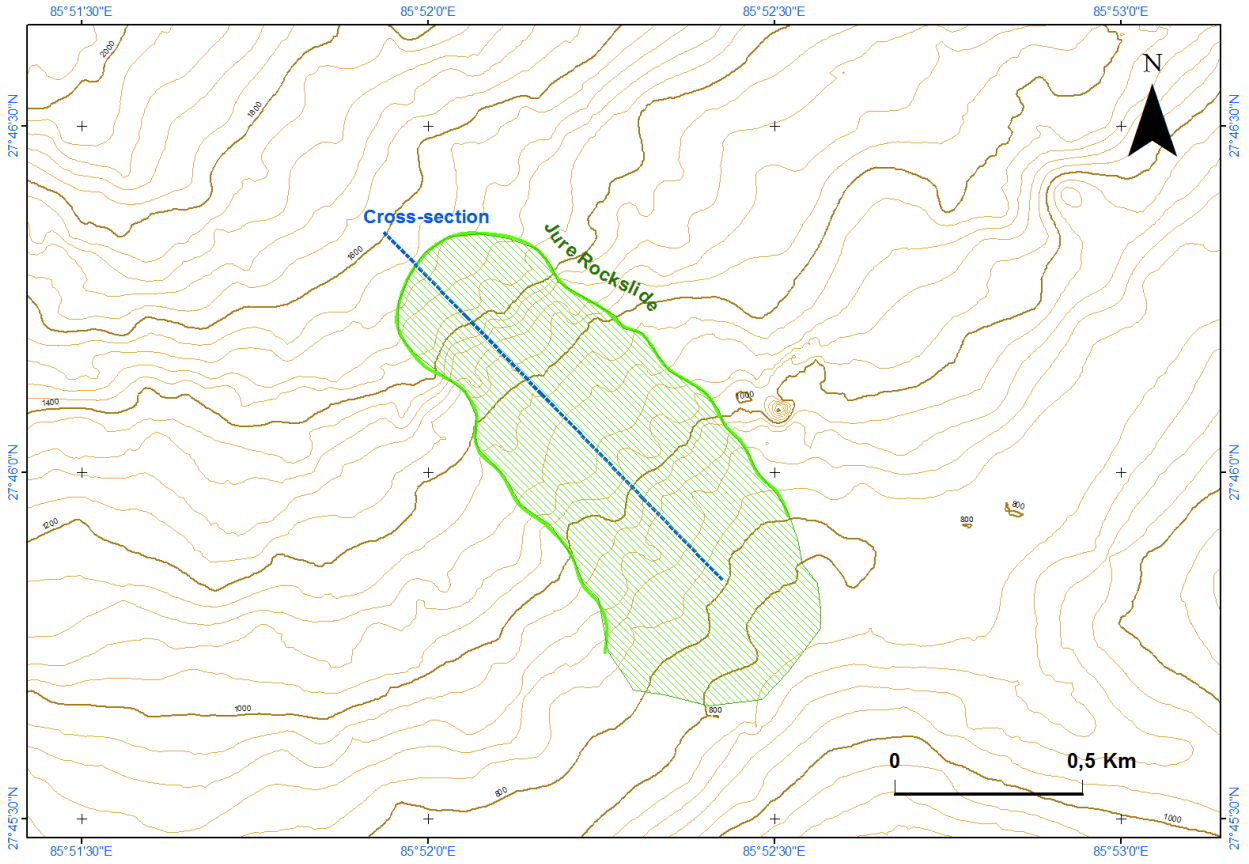

Figure 6.1: Topographic map after Jure rockslide. The selected cross section and the outline of the Jure rockslide are shown. Modified from GoogleEarth (2016).

In addition to the major discontinuity set, other input parameters are:

- **Dip/Dip Direction** of natural slope = 42°/135° (from Google Earth and Topographic map of the site before disaster shown in figure 7.1)
- **Friction Angle,** $\phi = 25°$ (from tilt test, Grøneng and Nilsen (2009))

Here, since it is a failed case, the residual friction angle ϕ_r should have been used which is related to the basic friction angle (ϕ_b) according to Barton and

Choubey (1977) by:

$$\phi_r = (\phi_b - 20) + 20\left(\frac{r}{R}\right) \tag{6.1}$$

where,

r = Schmidt rebound number on wet and weathered fracture surfaces

R = Schmidt rebound number on dry unweathered sawn surfaces

Due to the lack of Schmidt rebound data from the field and also since ϕ_b is nearly equal to ϕ_r according to Hoek (2000), the basic friction angle (ϕ_b) has been used as the input for the friction angle in this case.

6.1.2 Analysis Results

Here, this situation fulfills the condition required for a plane failure (figure 3.2) which is:

$$\psi_f > \psi_p > \phi \tag{6.2}$$

Also, a stereonet for this condition is plotted using DIPS which analyzes five different failure modes; namely Planar Sliding, Planar Sliding (No Limits), Wedge Sliding, Flexural Toppling and Direct Toppling.

The output from DIPS also confirms that Jure rockslide was a plane failure case. The results for planar sliding is illustrated in figure 6.2. In the figure, the crescent-shaped zone formed by the Daylight Envelope and the pole friction circle indicates the critical region of planar sliding which is highlighted in light red color. Theoretically, any poles in this region represent planes which can and will slide. However, in real life situations, it has been seen that planar sliding (and top-

pling) tends to happen when the dip direction of planes is within a certain angular range of the slope dip direction. Normally, a range of ±20° or 30° is considered, and poles outside of this range represent a low risk of plane failure (Hudson and Harrison, 2000).

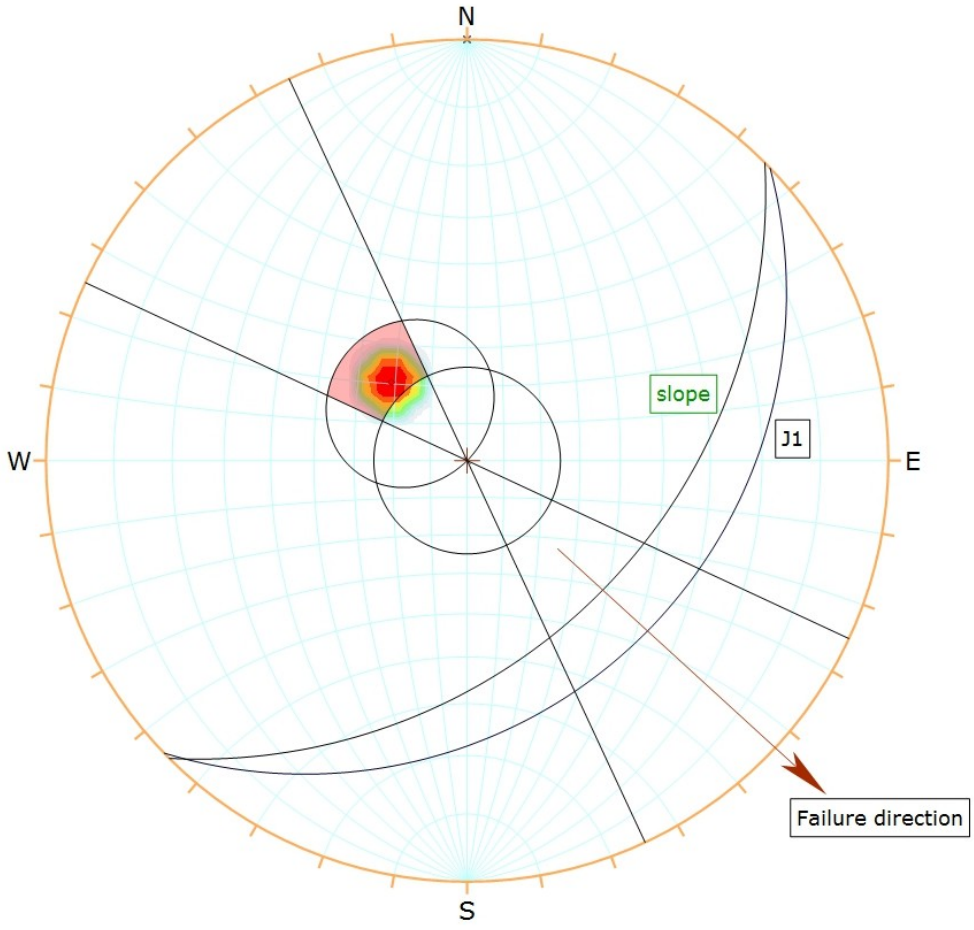

Figure 6.2: DIPS output: Plane failure (with 20° lateral limits)

For this case, the value of ±20° has been used for the lateral limits as shown in figure 6.2. The direction of the sliding failure is also illustrated in the figure above.

6.2 Limit Equilibrium Method (LEM)

As described in chapter 4.2.2, back calculation method is used in LEM to determine the shear strength parameters of Jure rockslide.

6.2.1 Assumptions

The assumptions made in plane failure analysis according to Wyllie and Mah (2004) are as follows:

- Both the tension crack and the sliding surface strike parallel to the slope.
- z_w is the depth of water filled up in the vertical tension crack.
- Water in the tension crack seeps through the base along the sliding surface and escapes through the daylighting portion of the slope face at atmospheric pressure. The hydrostatic pressure distribution in the tension crack and along the sliding surface are shown in figure 6.3.
- All three forces; namely W (the weight of the sliding block), U (uplift force due to water pressure on the sliding surface) and V (force due to water pressure in the tension crack), act through the centroid of the sliding mass. This means that there are no moments involved, and thus the failure is by sliding only.
- There is the presence of the release surfaces which offer no resistance to sliding at the lateral boundaries of the failing rock mass (Figure 3.2(b))

6.2.2 Back Calculation

For the back calculation, the geometry of the slope as calculated from the topographic map are as follows (Refer figure 6.3):

Here,

Slope height, H = 120 m

Slope angle, $\psi_f = 41.67°$

Inclination of potential failure plane, $\psi_p = 29.30°$

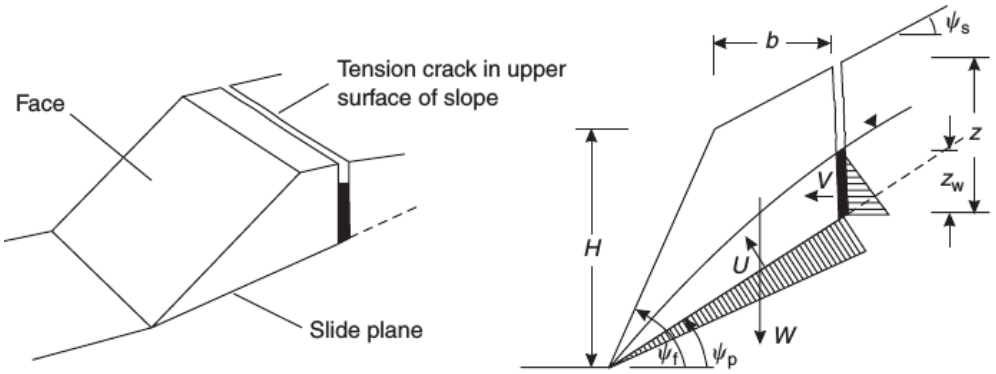

Figure 6.3: Slope geometries and ground water conditions for back calculation (Wyllie and Mah (2004))

Since the exact location of the tension crack is hard to measure from Google Earth, the critical tension crack depth and location has been calculated in case of a dry slope as recommended in Wyllie and Mah (2004) by the formulae:

$$\frac{z_c}{H} = 1 - \sqrt{cot\psi_f tan\psi_p} \tag{6.3}$$

where,

z_c = critical tension crack depth for a dry slope

and,

$$\frac{b_c}{H} = \sqrt{cot\psi_f cot\psi_p} - cot\psi_f \tag{6.4}$$

where,

b_c = distance of critical tension crack from the tip

The values of z_c and b_c are substituted for depth of tension crack (z) and distance of tension crack from the tip (b) as referred in figure 6.3. Hence, z and b are calculated to be 24.71 m and 35 m respectively.

From those dimensions and taking the unit weight of rock (γ_r) as 25.76 kN/m³ as found from laboratory test, the weight of the sliding mass is calculated to be **244.6 MN/m** using the formula

$$W = \gamma_r[(1 - cot\psi_f tan\psi_p)(bH + \frac{1}{2}H^2 cot\psi_f) + \frac{1}{2}b^2(tan\psi_s - tan\psi_p)] \tag{6.5}$$

With regards to the seismic load, the maximum earthquake load which is an equivalent horizontal load, generally representing the most unfavorable condition for stability, can be expressed as:

$$F_\alpha = \alpha.\frac{W}{g} \tag{6.6}$$

where,

α = maximum seismic acceleration denoted in a fraction of g

g = acceleration due to gravity in m/sec^2

In this analysis, no seismic force (F_α = 0) is assumed as there was no seismic event before the failure.

For deterministic limit equilibrium analysis, Factor of Safety (FOS) is defined by Wyllie and Mah (2004) as:

$$FOS = \frac{\text{Stabilizing Forces}}{\text{Driving Forces}} \tag{6.7}$$

For the dry condition, i.e. height of water in tension crack, $z_w = 0$, FOS is defined by:

$$FOS = \frac{cA + W cos\psi_p tan\phi}{W sin\psi_p} \tag{6.8}$$

where,

c = cohesion

A = area of sliding plane, given by

$$A = \frac{H + b tan\phi_s - z}{sin\psi_p} = 385 m^2/m \tag{6.9}$$

For the back calculation, the factor safety is set at 1 for the dry slope which represents the "just-failure case" which transforms equation 6.8 to

$$108224.16 = 342.50 * c + 192853.19 * tan\phi \tag{6.10}$$

Equation 6.10 is a linear equation with two variables which means that multiple combinations of c and ϕ are valid for the failure case.

Putting c=0 in equation 6.10 gives ϕ value as 29.3° which is also known as active friction angle (ϕ_a) which is related to the shear strength by the following relationship:

$$\tau = \sigma_n tan\phi_a \tag{6.11}$$

where,

τ= shear strength of joint

σ_n = normal stress, given by the equation:

$$\sigma_n = \frac{W cos\psi_p}{H/sin\psi_p} \tag{6.12}$$

From equations 6.11 and 6.12, τ_n and σ_n are calculated to be 0.6 MPa and 1.1 MPa respectively.

In this case without water and seismic forces, ϕ_a is equal to the slope of potential failure plane (ψ_f) which can also be found out from equation 6.8 by assigning FOS as 1 and c as 0.

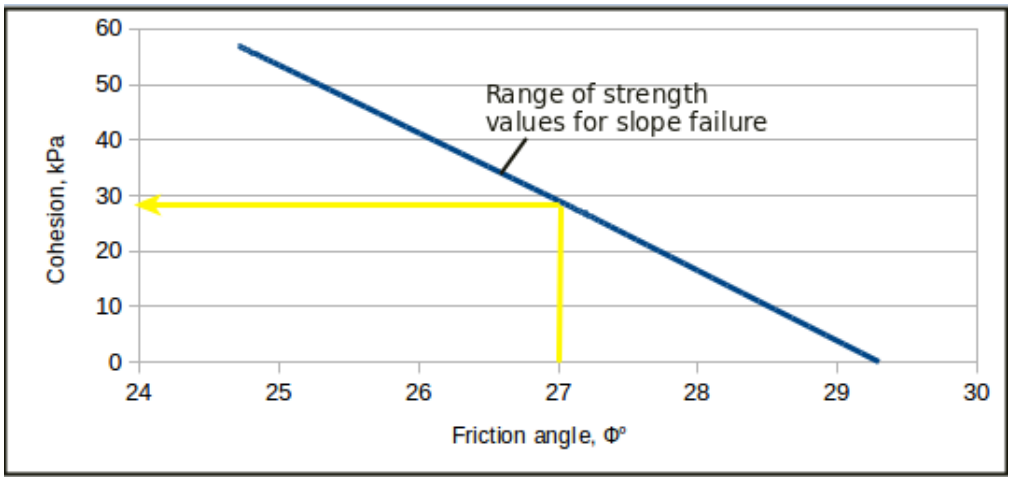

Figure 6.4: Mobilized shear strength for slope failure

From equation 6.10, a graph is plotted as shown in figure 6.4. As ϕ cannot be less than ϕ_b and not more than ϕ_a, the range of ϕ is ascertained to be from 24.7° to 29.3°. As shown in the figure, at a friction angle of 27°, the corresponding cohesion value is 29 kPa, and for higher friction angles, the required cohesion is reduced. Hence, the chosen cohesion and friction angle are 29 kPa and 27°

respectively which are later used as input for Phase² model in chapter 7.

6.2.3 Sensitivity Analysis

Moreover, a sensitivity analysis is carried out with the varying groundwater level. The main aim of this analysis is to study the influence of the groundwater level on the stability of the slope. The level of water in the tension crack is varied from 0% (dry case) up to 100% (fully saturated case) and the corresponding factor of safety is calculated.

The factor of safety when water is present is calculated from the formula:

$$FOS = \frac{cA + [Wcos\psi_p - U - Vsin\psi_p]tan\phi}{Wsin\psi_p + Vcos\psi_p} \tag{6.13}$$

where,

U = Resultant water pressure, given by

$$U = \frac{1}{2}\gamma_w z_w \frac{(H + btan\psi_s - z)}{sin\psi_p} \tag{6.14}$$

and, V = Water forces acting in the tension crack, given by

$$V = \frac{1}{2}\gamma_w {z_w}^2 \tag{6.15}$$

The results of the sensitivity analysis are shown in figure 6.5. As seen, the factor of safety decreases up to 0.76 when the tension crack is fully filled with water. These results indicate that even if the slope is considered safe in dry condition, the introduction of water largely decreases the stability of the slope.

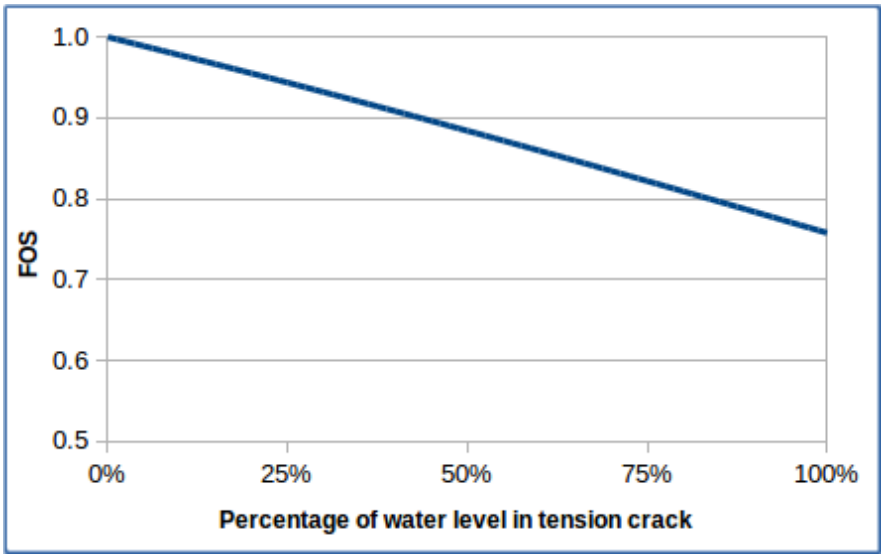

Figure 6.5: Sensitivity analysis with varying water level in tension crack

6.2.4 Determination of Barton-Bandis Shear Strength Parameters

Furthermore, the Barton-Bandis shear strength parameters are also estimated from back calculation. The empirical relationship according to Barton (1973) is given as

$$\tau = \sigma_n tan\left[JRClog_{10}\left(\frac{JCS}{\sigma_n}\right) + \phi_b\right] \tag{6.16}$$

where,

JRC = Joint Roughness Coefficient

JCS = Joint-wall Compressive Strength

Comparing equations 6.11 and 6.16, we get,

$$\phi_a = JRClog_{10}\left(\frac{JCS}{\sigma_n}\right) + \phi_b \tag{6.17}$$

According to Barton and Choubey (1977), JCS will be equal to the unconfined compressive strength of the unweathered rock mass if the joints are completely unweathered. Following the ISRM (2007b) standards, the value of compressive strength of intact rock is determined in the laboratory to be 84.9 MPa. Then, the compressive strength of rock mass is calculated from the formula given by Panthi (2006):

$$\sigma_{cm} = \frac{{\sigma_{ci}}^{1.5}}{60} \tag{6.18}$$

where

σ_{cm} = compressive strength of the rock mass

σ_{ci} = compressive strength of intact rock

From equation 6.18, σ_{cm} (= JCS) is calculated to be 13 MPa.

Then, from equation 6.17, JRC is estimated to be equal to 4. These Barton-Bandis shear strength parameters are also used as input for numerical modeling in chapter 7.

Chapter 7

Numerical Analysis of Jure Landslide

For the numerical analysis, the Phase² 2D finite element numerical modeling tool has been used as already described in Chapter 4.3. This is the last step of the slope stability analysis of the Jure rockslide.

7.1 Input for Numerical Modeling

The most important aspect of obtaining a suitable numerical model is the quality of the input data. In this study, the input data used can be broadly classified into two categories as described in the sub-sections below.

7.1.1 Laboratory Work

The laboratory experiments were conducted on different days between January and March 2016 strictly following the ISRM and NTNU/SINTEF standards. The rock sample was collected from the Jure rockslide deposits during the field work in summer 2015. From the mineralogical composition, it has been found out that the sandstone sample contained 63% quartz, 24% albite, 10% muscovite

and 3% chlorite. Table 7.1 lists the standards used in the laboratory testing procedures.

Table 7.1: Laboratory Test Standards

S. No.	Parameter	Test	Reference
1	Basic friction angle (ϕ_b)	Tilt Test	Grøneng and Nilsen (2009)
2	Uniaxial Compressive Strength (σ_{ci})	UCS Test	ISRM (2007a)
3	Young's Modulus (E_i)	UCS Test	ISRM (2007b)
3	Tensile strength (σ_t)	Brazil Test	ISRM (1978)

The values of the parameters obtained are shown in table 7.2:

Table 7.2: Laboratory Test Results

S. No.	Parameter	Value
1	ϕ_b	24.7°
2	σ_{ci}	84.9 MPa
3	E_i	32636 MPa
4	σ_t	9.42 MPa

Apart from those parameters in table 7.2, Poisson's ratio (ν) is calculated to be 0.47 which was too high and cannot be taken as a reliable parameter for the analysis. So instead, 0.15 is taken as an appropriate value for further calculations following Panthi (2006) where the mean value of metasandstone samples collected from Nepal was calculated to be 0.14.

7.1.2 Discontinuity Shear Strength Parameters

The shear strength parameters of discontinuity J_1 are estimated from Barton-Bandis empirical method (Barton and Choubey, 1977). According to Barton-Bandis, the shear strength parameters are joint roughness coefficient (JRC), joint compressive strength (JCS) and residual friction angle (ϕ_r).

JRC

JRC is an empirical index used for the characterization of the surface roughness. It was calculated by back calculation as described in chapter 6.2.4.

JCS

JCS is an index representing the strength of the rock at the discontinuity surface. It was assumed to be equal to the compressive strength of the rock mass and calculated as described in chapter 6.2.4.

Basic friction angle (ϕ_b) and residual friction angle (ϕ_r)

According to Grøneng and Nilsen (2009), the basic friction angle (ϕ_b) is considered as a material constant referring to smooth, planar surfaces in fresh rock whereas the residual friction angle (ϕ_r) relates to the residual properties of natural joint surfaces after shear displacement.

In this study, ϕ_b is determined with tilt test in the laboratory, following Grøneng and Nilsen (2009) standards. Three samples have been tested, and the tilt angle (=ϕ_b) is calculated. The calculation is attached in Appendix A.

According to Barton (1973), ϕ_r for natural joints can be assumed equal to ϕ_b or

the tilt angle for sawn surfaces of the same rock material. This assumption is used for the discontinuities in the Jure rock mass. Thus, $\phi_r = \phi_b = 24.7°$ is assumed as the input value.

The summary of the input values regarding Barton-Bandis shear strength parameters are tabulated in Table 7.3.

Table 7.3: Barton-Bandis Shear Strength Parameters

S. No.	Parameter	Value
1	JRC	4
2	JCS	13 MPa
3	ϕ_b	24.7°

Joint Stiffness

In Phase², the joint stiffness parameters should also be used as the input. The normal stiffness (k_n) and shear stiffness (k_s) of joint are calculated following Rocscience (2016b) help, based on the following equations:

$$k_n = \frac{E_i E_m}{L(E_i - E_m)} \tag{7.1}$$

where,

E_i = intact rock modulus (Table 7.2)

E_m = rock mass modulus (Equation 6.18)

L = mean joint spacing = 1 m

Similarly,

$$k_s = \frac{G_i G_m}{L(G_i - G_m)} \tag{7.2}$$

where,

G_i = intact rock shear modulus (Table 7.2)

G_m = rock mass shear modulus (Equation 6.18)

According to Shrestha and Panthi (2013), the shear modulus is related to normal modulus by the relation:

$$G = \frac{E}{2(1+\nu)} \tag{7.3}$$

Hence, from equations 7.1 and 7.2, k_n and k_s are calculated to be 5921.18 MPa/m and 2574.43 MPa/m respectively.

7.2 Model Setup

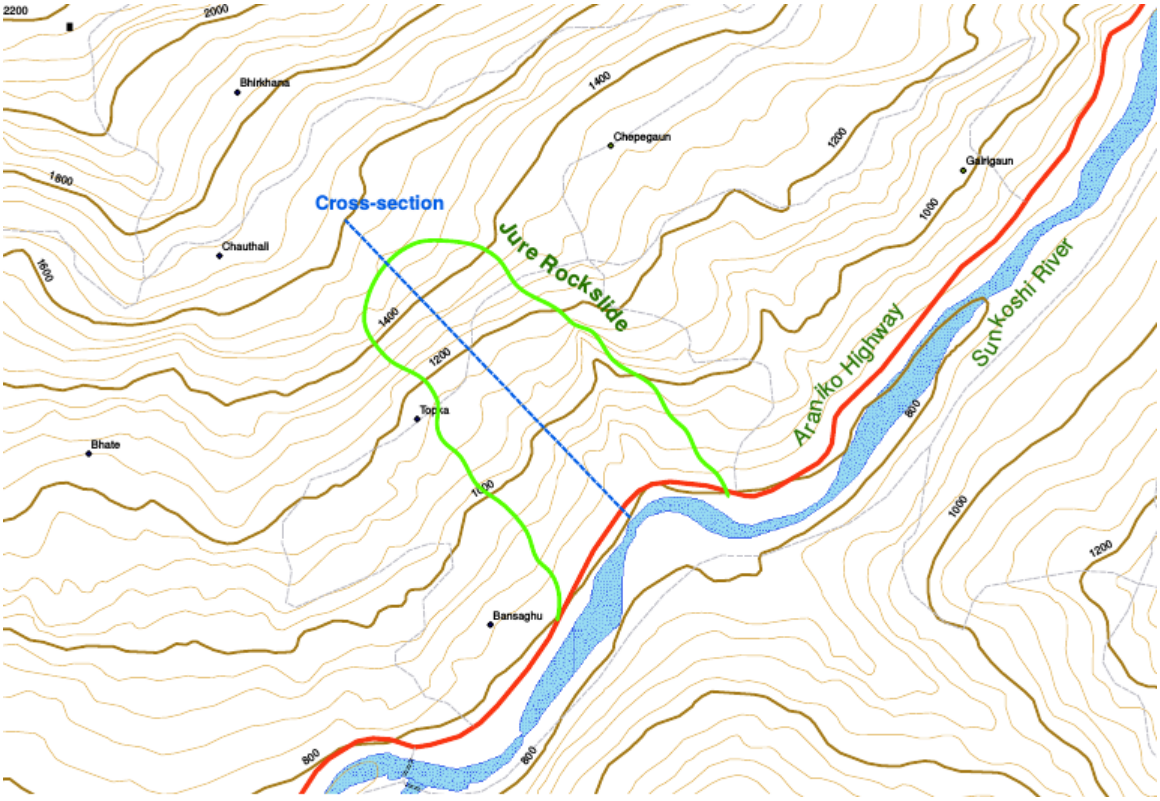

Figure 7.1: Topographic map of Jure site before disaster with the chosen cross-section. (Modified from Survey Department, Ministry of Land Reform and Management, Nepal.)

A 2-dimensional, one stage model is constructed for the numerical modeling of Jure rockslide. The model is built based on the cross section profile of the topography of Jure rockslide before disaster as shown in figure 7.1.

The location of the profile is chosen through more or less the center of the rockslide, illustrated as a blue line in the figure, which is assumed the most active part of the slope regarding the slope deformation. The profile is oriented perpendicular to the valley slope and rises from the level of Araniko Highway at 800 m.a.s.l up to the top of the hill slope at 1600 m.a.s.l.. Also, the main joint set J1 is also assigned which is dipping at an angle of 29° as shown in figure 7.4.

Boundary Setup

The chosen profile size is based on recommendations by Wyllie and Mah (2004) (Refer Figure 7.2) in order to avoid boundary effects, as artificial boundaries are non-existent in real world scenarios.

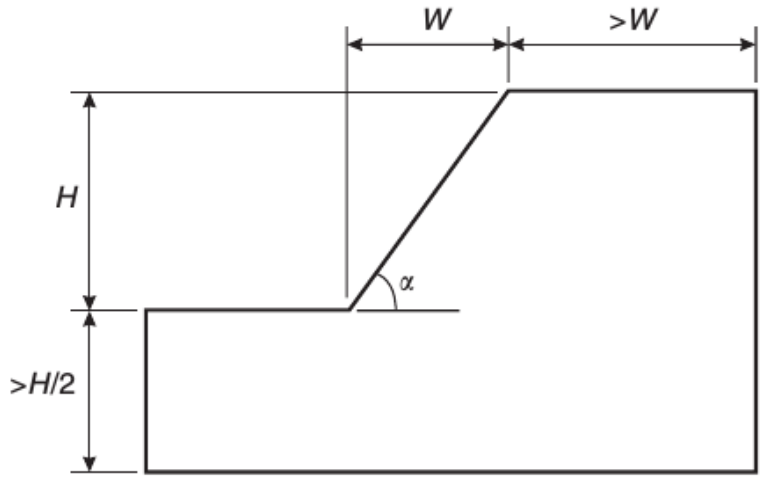

Figure 7.2: Typical recommendations for locations of artificial boundaries in slope stability analyses (Wyllie and Mah, 2004).

If the artificial boundaries are located too close to the area with the slope sta-

bility problem in the model, they may influence the analysis by pre-described displacement, or stress (Wyllie and Mah, 2004).

Table 7.4 gives an overview of the general boundaries set up of the Phase² model.

Table 7.4: Boundary Setup for Phase² model

Boundary	Condition	Recommendation
Ground Surface	Free to move in all directions	Rocscience (2016b)
Base and left & right boundaries	Restrain X, Y	Rocscience (2016b)

Mesh Setup

A graded mesh consisting of 3-noded triangular elements with default number of nodes on external is chosen for the model. The selected settings give a quick modeling and still gives satisfactory computation results. An attempt to increase the number of nodes and/or changing to 6-noded triangular elements have been also tried but did not yield noticeable difference in results even with far much longer computation time. The mesh density is increased in the area of concern regarding slope instability to produce better results. This is assumed to give the most representative analysis in the search for a most probable sliding plane.

Elastic and Plastic Material

Mohr-Coulomb failure criterion uses peak shear strength to depict failure within the rock mass (figure 7.3). The peak strength parameter describes failure in case of elastic rock mass whereas the residual values in plastic. After the peak value is obtained, the shear stress will eventually reach some residual value which will

stay constant even for further displacements (Wyllie and Mah, 2004).

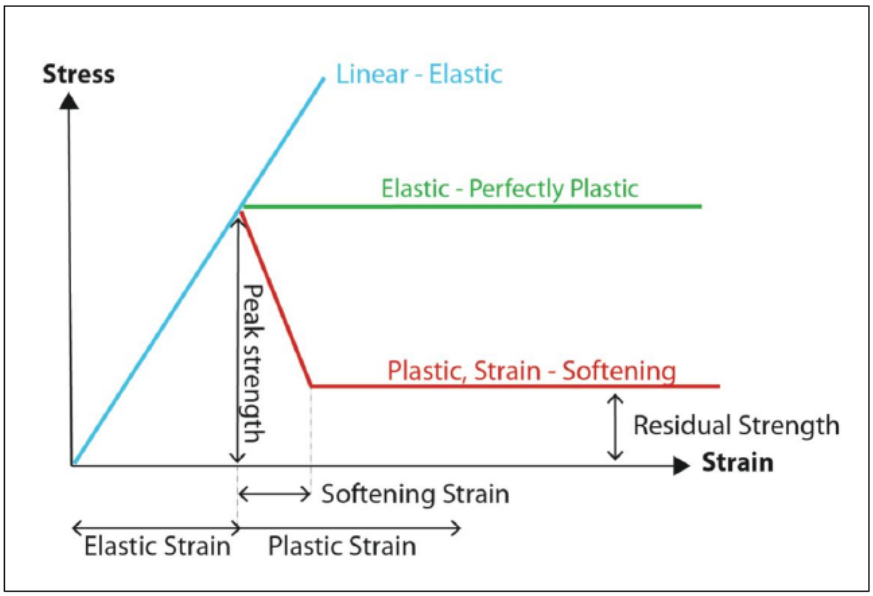

Figure 7.3: Stress – Strain relationship which represents the rock mass behavior when considering different material models (Sandøy, 2012).

Phase² allows elastic and/or plastic analysis of slope stability. For the Jure rockslide, both elastic-perfectly plastic model (residual values = peak values) and plastic, strain softening model (residual values = 10% of peak values) are run separately. The stress-strain relatinship of different rock mass behavior is shown in figure 7.3

Failure Criterion

In Phase², there are several failure criteria to choose from. The Mohr-Coulomb failure criterion is selected for this analysis to make use of the cohesion and friction angle found by back calculation by LEM as described in chapter 6.2.

Tension Cracks

According to Rocscience (2016b), Phase² does not permit the users to model tension cracks directly because there are no facilities in the finite-element method to assign zero strength to a material and at the same time apply possible hydrostatic forces to the crack surfaces. Hence, to avoid further uncertainties, no tension cracks have been attempted to be incorporated into the model.

Final Model

Applying the above-mentioned settings, a final profile model was generated as shown in figure 7.4.

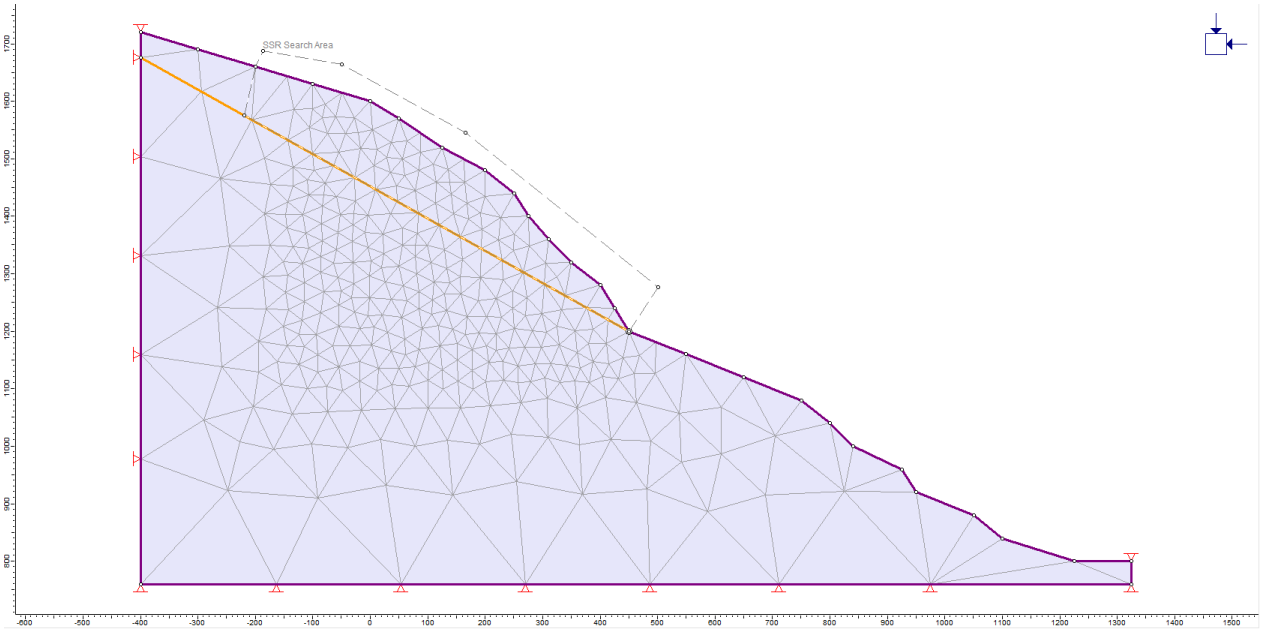

Figure 7.4: Final Phase² profile of Jure rockslide with SSR search area

For analyzing the failure, very high groundwater conditions are incorporated in the Phase² model. The continuous rainfall during the period before the disaster might have obviously increased the groundwater table. The assumption of

the high water table is also justified from the fact that small streams are running from the top of the hillslope in the site as observed during the fieldwork in summer 2015.

Since, there are no piezometric readings of the site, finite element groundwater analysis is carried out at first to determine the water table in the model, and then the model is further run to perform the stress analysis. The boundary conditions for carrying out the finite element groundwater analysis are shown in table 7.5.

Table 7.5: Boundary Setup for Finite Element Groundwater Analysis in Phase² model

Boundary	**Condition**
Ground Surface	Unknown (P=0, Q=0)
Left Side	Fixed Total Head, H= 1700 m
Right Side	Fixed Total Head, H= 800 m

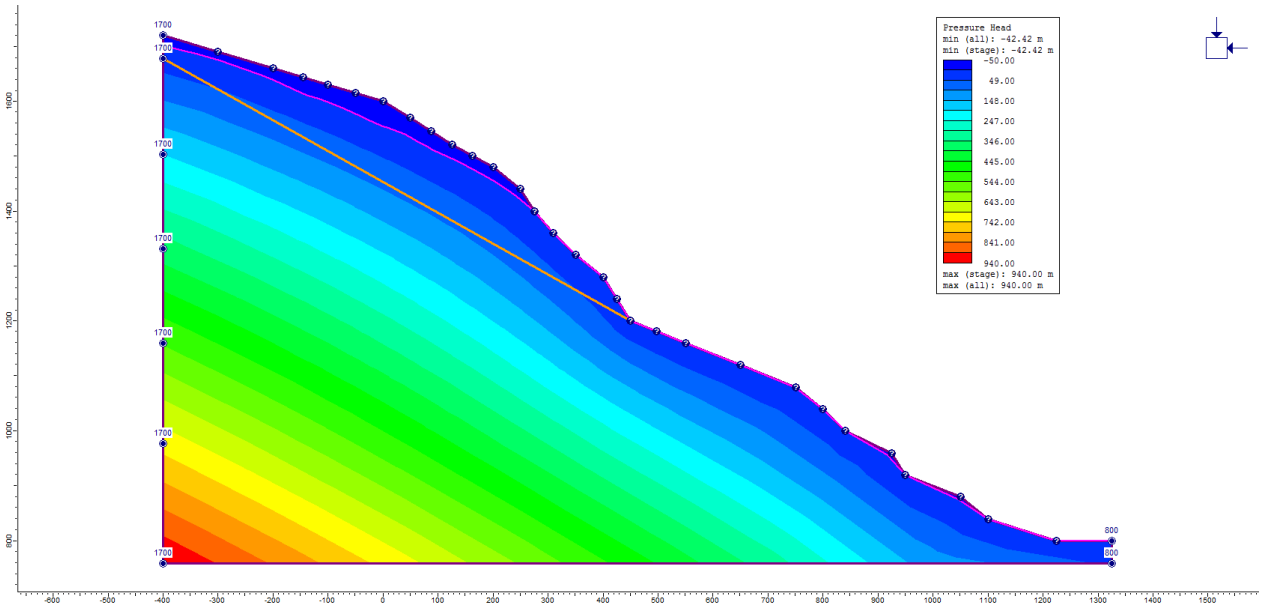

Figure 7.5: Result of finite element groundwater analysis used as an input for stress computations. The pink line shows the computed water table.

The result of finite element groundwater analysis is shown in figure 7.5 with the assigned boundary conditions. Also, the computed water table is shown by a pink line which runs close to the ground surface.

7.3 Summary of scenarios

The Phase2 analyses are conducted through a total of 4 main analyses. An overview is listed below:

- **Analysis 1:** Elastic – perfectly plastic model, peak values equal residual values, in dry condition.
- **Analysis 2:** Strain softening model (residual = 10% of peak friction angle and cohesion) in dry condition.
- **Analysis 3:** Elastic – perfectly plastic model, peak values equal residual values, in high groundwater condition.
- **Analysis 4:** Strain softening model (residual = 10% of peak friction and cohesion) in high groundwater condition.

Analyses 1 and 2 represent the ***"before failure"*** situation while analyses 3 and 4 are supposed to represent the ***"after failure"*** situation.

7.4 Phase^2 Results

The numerical modeling results are broadly classified into two categories, maximum shear strain and displacement to compare both, before failure and after

failure, conditions.

7.4.1 Maximum Shear Strain

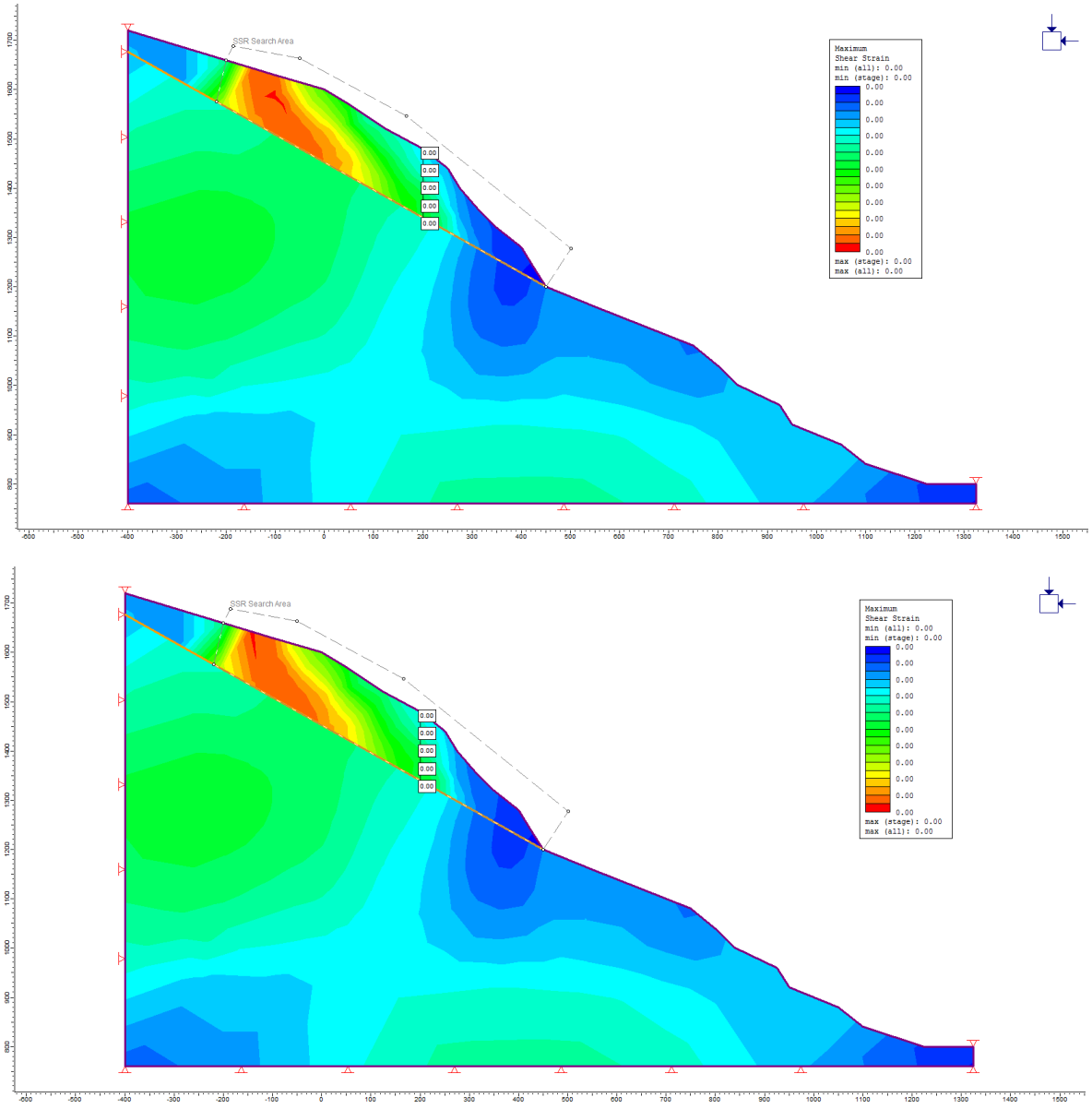

Figure 7.6: Maximum shear strain results for dry cases; (UP) Analysis 1 and (DOWN) Analysis 2.

The maximum shear strain results from the dry cases show an accumulation of high strain in the top face of the Jure slope as shown in figure 7.6. This can

be compared to the formation of tension cracks in the slope face as mentioned earlier in chapter 2.4.

On the other hand, for the high groundwater cases (or after failure cases), the shear strain is seen more accumulated mostly in the joint boundary as shown in figure 7.7.

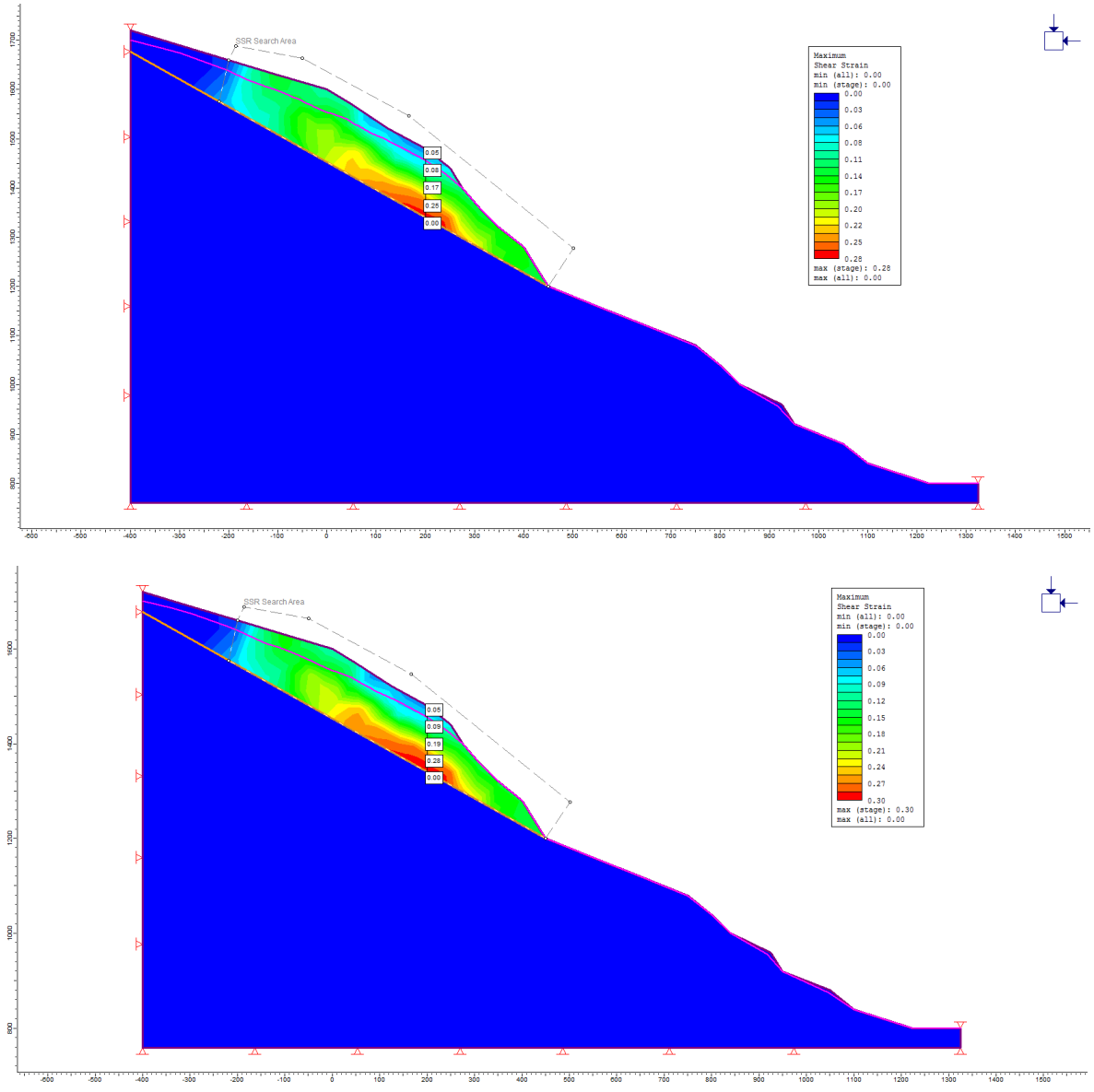

Figure 7.7: Maximum shear strain results for high groundwater cases; (UP) Analysis 3 and (DOWN) Analysis 4.

7.4.2 Displacement

For the dry cases, the total displacements seen are small and mostly concentrated on the top face of the slope where the pre-failure movements were observed as explained earlier in chapter 2.4. The maximum displacement for analysis 1 and 2 are found to be 0.03 m and 2.74 m respectively as shown in figure 7.8.

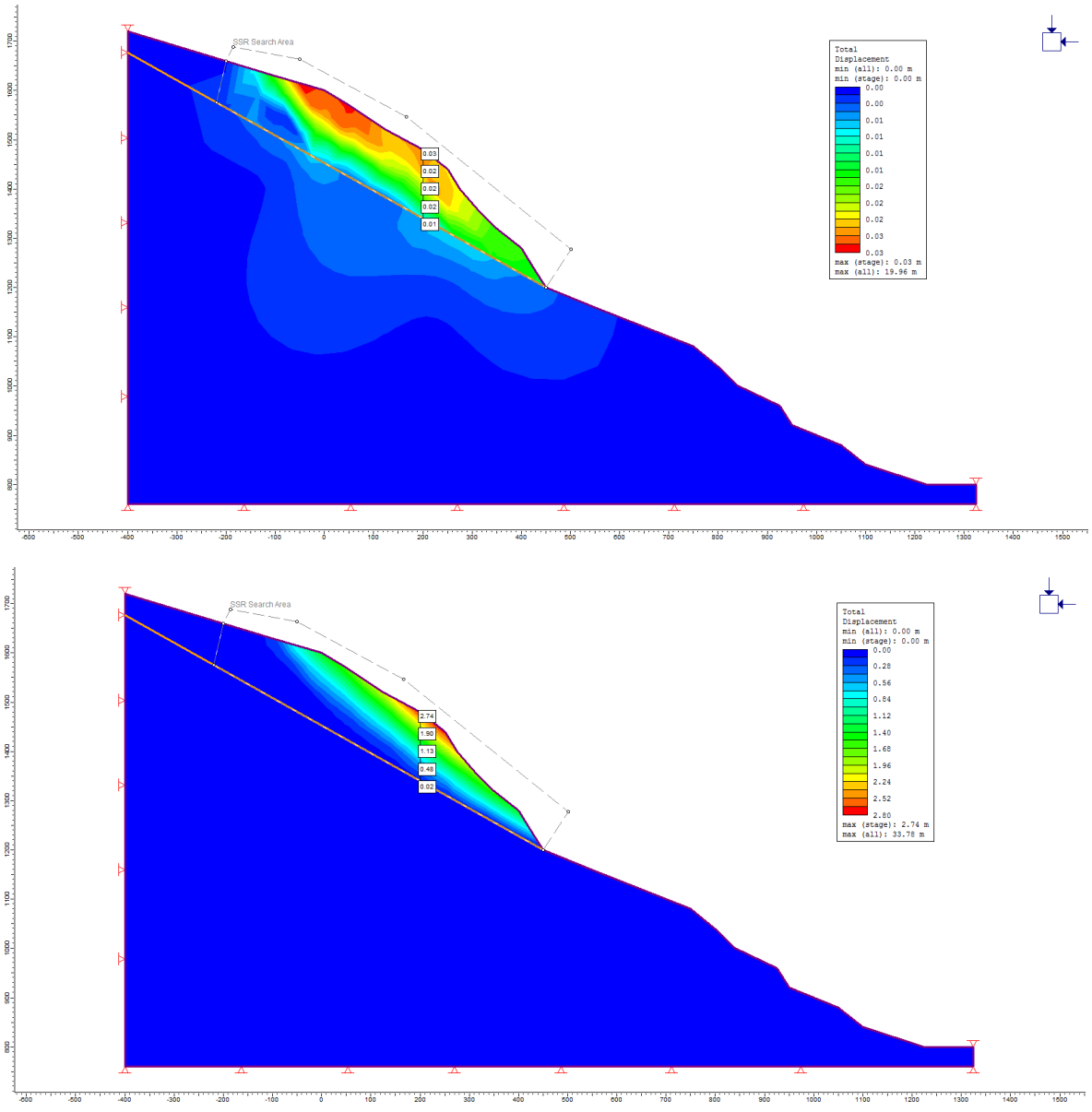

Figure 7.8: Total displacement for dry cases; (UP) Analysis 1 and (DOWN) Analysis 2.

On the other hand, for the wet cases, much higher values than the dry cases are observed in the total displacement results as shown in figure 7.9. The maximum values are 30.52 m and 36.48 m for analyses 3 and 4 respectively. This shows that the increase of the groundwater table triggers more movement of the slope.

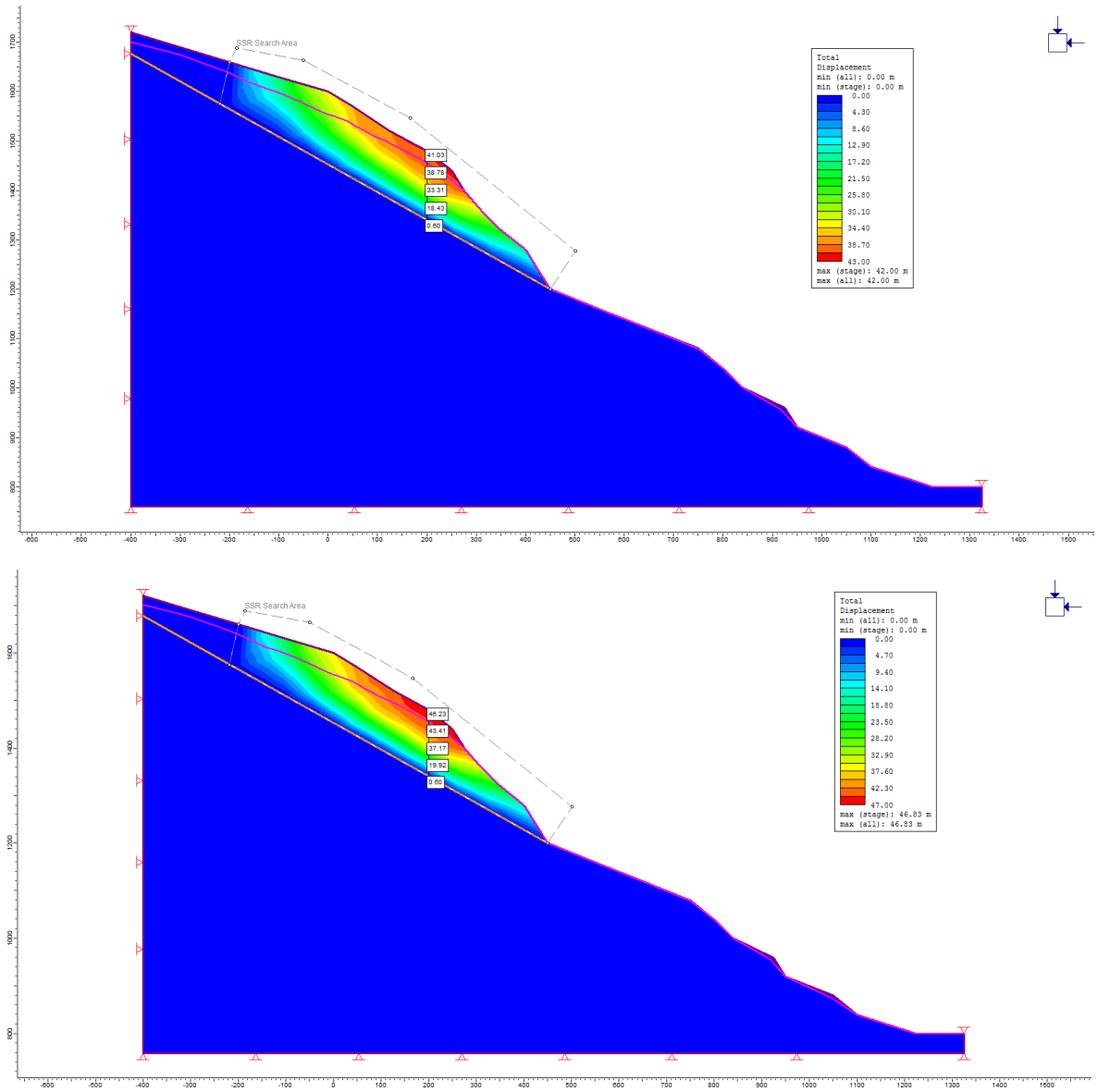

Figure 7.9: Total displacement for high groundwater cases; (UP) Analysis 3 and (DOWN) Analysis 4.

7.5 Discussion of Stability Analysis Results

The overall stability analysis results are aimed at a better understanding of the actual slope failure process. The kinematic analysis confirms the Jure rockslide as a planar slide. Through the back calculation using limit equilibrium, the shear strength parameters of the rock mass (c & ϕ) are calculated. Moreover, the sensitivity analysis is also done to analyze the the sensitiveness of the groundwater conditions in the slope failure. It shows that a stable slope would be converted into a far more unstable slope when the groundwater level is raised.

The numerical model of the rockslide also shows the formation of the tension cracks and some movements in the slope face in the dry case. After the raising of the water table (to simulate the monsoon situation), it shows far more displacements which can lead to the sudden failure. Hence, it is concluded that the groundwater condition is the principal cause of the failure which coupled with the major discontinuity set to produce a massive sliding failure.

In this study, a simplified model has been chosen for slope stability analysis. However, the actual rockslide might be far too complicated. Other subsidiary discontinuities, induced rock stresses, fault zones, among others might have also assisted in the failure apart from the groundwater conditions and the major discontinuity set. But, nevertheless, this study was primarily aimed to observe the effects of groundwater on a stable hill slope.

Chapter 8

Earthquake Impacts on the Sunkoshi Valley

8.1 Salient Features of HPPs along the Sunkoshi Valley

The salient features of the eight hydropower projects located in the Sunkoshi Valley as shown in 2.3 are shown in table 8.1.

Table 8.1: Salient features of HPPs along Sunkoshi Valley

S. No.	Name	Capacity (MW)	Type	Status
1	Bhairabkunda	3	ROR	Completed
2	Upper Bhotekoshi	45	ROR	Completed
3	Upper Chaku "A"	22.2	ROR	Under Construction
4	Middle Chaku	1.8	ROR	. Completed
5	Chaku Khola	3.00	ROR	Completed
6	Lower Chaku	1.765	ROR	Completed
7	Sunkoshi Small	2.5	ROR	Completed
8	Sunkoshi	10.05	ROR	Completed

8.2 Earthquake Damage Details on HPPs

This section briefly describes the damages on the eight hydropower projects mentioned above due to the Gorkha earthquake and its aftershocks.

8.2.1 Bhairabkunda HPP

During the earthquake, there was a substantial damage in the intake due to rock and debris fall. The headrace tunnel suffered leakage and also the penstock was burst. Moreover, the switchyard and the transmission line were damaged, but the powerhouse was safe.

Figure 8.1: (LEFT) Debris fall in the intake area of Bhairabkunda HPP. (Photo Credit: Surya Thapa/Bhairabkunda HPP) (RIGHT) Penstock, powerhouse, and switchyard of Bhairabkunda HPP. The penstock and the switch yard were heavily damaged.

8.2.2 Upper Bhotekoshi HPP

Upper Bhotekoshi HPP, which is also the largest of those above eight, suffered the most damages of all. The earthquake induced the rockfall in the cliff right above the penstock which burst the penstock, due to which the powerhouse downstream was submerged. The project was shut down for about five months the previous year due to damages in the transmission lines due to the Jure rockslide on 2^{nd} of August 2014.

Figure 8.2: (LEFT) Penstock of Bhotekoshi HPP, which was burst due to the rockfalls from the cliffs in the background. (RIGHT) Scouring due to flooding after the penstock burst.

8.2.3 Upper Chaku "A" HPP

Since this under-construction project was inaccessible at the time of fieldwork, information was collected by personally interviewing Saroj Khanal, an engineer of the project. According to him, the penstock pipes were washed out by the debris fall and the incomplete powerhouse also received some damages.

8.2.4 Middle Chaku HPP

There were minor damages in the intake of Middle Chaku HPP but the powerhouse suffered more damages due to the shaking. Cracks were seen in the columns of the powerhouse due to the shaking. Minor rockfalls were observed nearby the powerhouse site.

Figure 8.3: Cracks seen in the powerhouse of Middle Chaku HPP. The damages seen are mostly due to the shaking.

8.2.5 Chaku Khola HPP

In Chaku Khola HPP, the penstock, powerhouse and staff quarters suffered minor damages due to the shaking as well as rockfall during the earthquake. The penstock was aligned along the surface of a cliff which suffered some dents from the rockfall. Some cracks were observed on the cliff on the right side as shown

in figure 8.4 which indicates that there is still a risk of shallow slope failures.

Figure 8.4: Powerhouse of Chaku Khola HPP with penstock in the background.

8.2.6 Lower Chaku HPP

Some minor damages were seen in Lower Chaku HPP due to the shaking. Also, the squeezing of the surface penstock aligned along the toe of the hil due to land subsidence was observed which was confirmed by lower production after the hiatus.

8.2.7 Sunkoshi Small HPP

The powerhouse of Sunkoshi Small HPP was submerged completely due to the dammed lake formed after the Jure rockslide the previous year. After recovering from that loss and when was ready to resume operations, the earthquake

struck, which caused substantial damage to the powerhouse structure. Moreover, the landslide caused more damages in the penstock alignment as well as in the headworks area.

Figure 8.5: Powerhouse of Sunkoshi Small HPP (inside the yellow circle) located on the banks of the Sunkoshi River. It was completely submerged due to the formation of a dammed lake because of Jure rockslide.

8.2.8 Sunkoshi HPP

The intake of the Sunkoshi Hydropower Project was damaged by sudden flooding after the release of water from the dammed lake caused by Jure landslide the previous year. To worsen the situation, the intake structure was damaged more due to the shaking. Moreover, the 3-km long headrace canal suffered multiple leakages apart from the damages in the staff quarters.

Figure 8.6: Intake of Sunkoshi HPP which bore the brunt of Jure rockslide as well as Gorkha Earthquake and the series of aftershocks.

8.3 Earthquake Induced Landslides in the Sunkoshi Valley

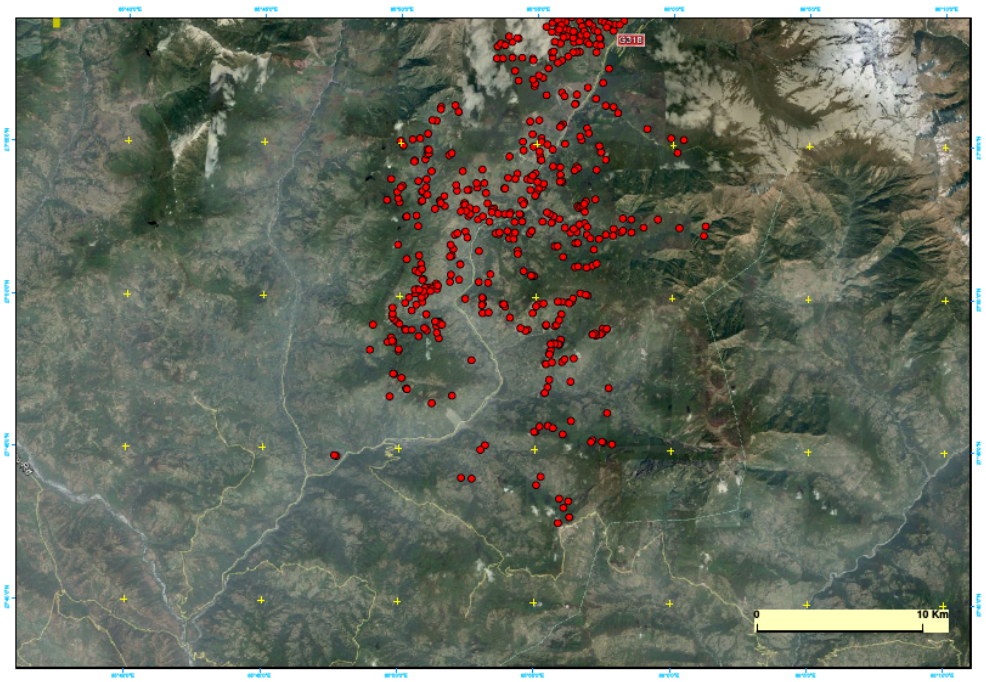

Figure 8.7: Earthquake-induced landslides in the Sunkoshi Valley. The red dots in the figure indicate landslides larger than 100 m. Data modified from DurhamUniversity (2015).

The map of landslides larger than 100 m in length (measured from the head to the toe) induced by the Gorkha earthquake and its aftershocks is shown in figure 8.7. The landslides were mapped by the staffs at Durham University and the British Geological Survey and latest data updated on 30^{th} of June 2015. The map clearly shows the denser clustering of such landslides in the northern areas of the Sunkoshi Valley near the Nepal-China border.

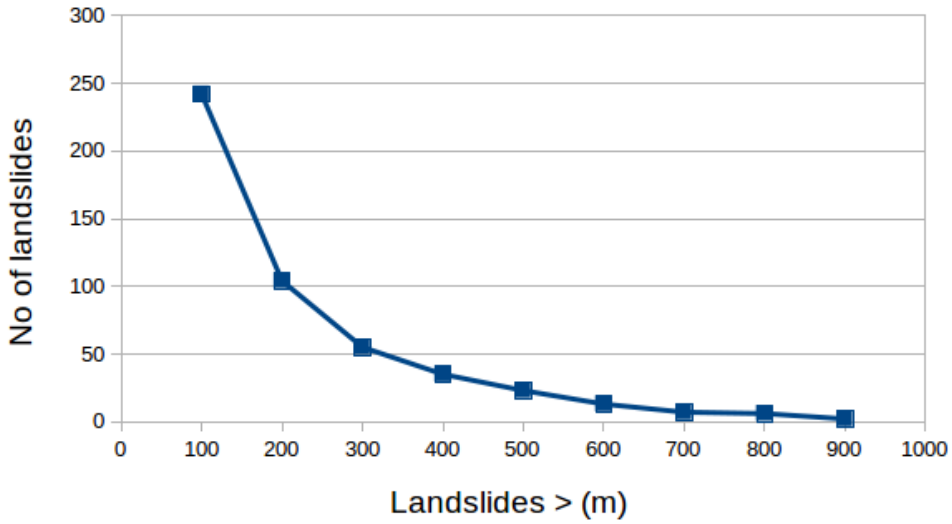

Figure 8.8: Distribution of >100 m landslides in the Sunkoshi Valley. Data modified from DurhamUniversity (2015).

Figure 8.8 shows that the total number of large landslides (classified by the length greater than 100 m) were 487 in toal. Those landslides are not only triggered by the Gorkha earthquake alone but also the combined effect of monsoon and earthquake or monsoon alone. This clearly shows the risks associated with the geology in the study area.

8.4 General Discussion on the Nature of the Damages

As mentioned in the previous sections, some similarities can be distinctly seen on the features of the hydropower projects and the nature of damages suffered. All of the projects have surface penstock and surface powerhouse. The loosely structured hill slopes could not bear the intense shaking of the Gorkha earthquake and its aftershocks, and hence, rock and debris fall was triggered. Most of the damages observed in the hydropower structures were more due to the secondary factors like the landslides than due to the shaking itself.
Moreover, the hill slopes which were weakened by the shaking were observed failing during the monsoon period (which was coincidently the fieldwork period). Many active landslides were seen with the frequent blocking of the roads and highways. More importantly, the earthquake and monsoon induced slope failures have been putting the lives of the local people in a constant threat.

8.5 Mitigation Measures

The following are the general mitigation measures to minimize the damages in the hydropower projects in the future:

- Proper geological studies should be carried out in the early stages of the formulation of the projects.

- Earthquake resistant design of the structures should be done strictly following the relevant codes.

- The underground alternatives for the structures (for example powerhouses

and headrace tunnels) should be properly assessed and chosen before the surface options whenever feasible technically as well as economically.

Chapter 9

Conclusions and Recommendations

9.1 Conclusions

The stability assessment of Jure rockslide has been carried out in three distinct steps, namely kinematic analysis, limit equilibrium and numerical modeling as described in chapter 4, 6 and 7. The analysis confirms the planar sliding failure in the upper portion of the rockslide. Furthermore, the failure conditions which have been assessed in the numerical modeling indicates that the high ground-water conditions and the orientation of the major discontinuity set J_1 are the major factors for the disaster. To summarize the slope stability assessment, it is concluded that the slope was just safe before the monsoon started. During the monsoon, the continuous addition of the weight of water caused the rock slope to slide along the main discontinuity set and caused a huge loss of life and property. The failure in the lower portion might be the secondary effect of the rapidly travelling mass of rock from the upstream although it is not analyzed in much details in this study.

Moreover, the observation of the earthquake damages in the hydropower projects

shows how vulnerable are the structures considering the fragile geology of the area. Since the Himalaya is relatively a younger rock, the nature of damages found in the Sunkoshi Valley can be comparable to other parts of Nepalese Himalayas with similar geology and topography. With the fact that Nepal is rapidly increasing its hydropower production in the recent times, the slope failures induced by the monsoon and/or earthquakes have reminded to consider detailed geological studies and adopt suitable designs for any projects in the future to reduce if not prevent the loss of lives and properties.

9.2 Recommendations for Further Work

The following are the recommendations for further work on this topic:

- The parameters obtained from the slope stability analyses can be compared with the field data to confirm if the model represented the actual site conditions.
- Both the portions of the Jure rockslide can be modeled to get a better overview of the failure conditions.
- Modeling can be done with other numerical modeling softwares for example RS3, FLAC2D, PLAXIS to name a few and compare with the results obtained from the Phase² model.
- The earthquake and monsoon-induced landslides can be investigated using Satellite Radar images.

References

Barton, N. (1973). Review of a new shear-strength criterion for rock joints. *Engineering Geology*, 7(4):287–332.

Barton, N. and Choubey, V. (1977). The shear strength of rock joints in theory and practice. *Rock Mechanics*, 10(1-2):1–54.

Champati Ray, P. K. and Chattoraj, S. L. (2014). Sunkoshi Landslide in Nepal and its possible impact in India: A Remote Sensing Based Appraisal. volume XL-8. The International Archives of the Photogrammetry, Remote Sensing and Spatial Information Sciences.

Dahal, R. K., Bhandary, N. P., Timilsina, M., Yatabe, R., and Hasegawa, S. (2013a). Earthquake-Induced Landslides in the Roadside Slopes of East Nepal After Recent September 18, 2011 Earthquake. In Ugai, K., Yagi, H., and Wakai, A., editors, *Earthquake-Induced Landslides*, pages 149–157. Springer Berlin Heidelberg. DOI: 10.1007/978-3-642-32238-9_16.

Dahal, R. K., Bhandary, N. P., Timilsina, M., Yatabe, R., and Hasegawa, S. (2013b). Earthquake-Induced Landslides in the Roadside Slopes of East Nepal After Recent September 18, 2011 Earthquake. In Ugai, K., Yagi, H., and Wakai, A., ed-

itors, *Earthquake-Induced Landslides*, pages 149–157. Springer Berlin Heidelberg. DOI: 10.1007/978-3-642-32238-9_16.

Dhital, M. R. (2015). Lesser Himalaya of Bagmati–Gosainkund Region. In *Geology of the Nepal Himalaya*, Regional Geology Reviews, pages 153–162. Springer International Publishing. DOI: 10.1007/978-3-319-02496-7_10.

DurhamUniversity (2015). Nepal Earthquake Landslide Locations, 30 June 2015 - Humanitarian Data Exchange.

Eberhardt, E. (2003). Rock Slope Stability Analysis - Utilization of Advanced Numerical Techniques.

Eberhardt, E. (2006). From Cause to Effect: Using Numerical Modelling to Understand Rock Slope Instability Mechanisms. In Evans, S. G., Mugnozza, G. S., Strom, A., and Hermanns, R. L., editors, *Landslides from Massive Rock Slope Failure*, pages 85–101. Springer Netherlands, Dordrecht.

ESRI (2016). ArcMap 10.3.

GoogleEarth (2016). Google Earth.

Griffiths, D. V. and Lane, P. A. (1999). Slope stability analysis by finite elements. *Géotechnique*, 49(3):387–403.

Grøneng, G. and Nilsen, B. (2009). Procedure for determining input parameters for Barton-Bandis joint shear strength formulation. Technical Report Internal Report no 38, Department of Geology and Mineral Resources Engineering, Norwegian University of Science and Technology.

Hammah, T Yacoub, B Corkum, F Wibowo, and JH Curran (2007). Analysis of blocky rock slopes with finite element Shear Strength Reduction analysis. In *Rock Mechanics: Meeting Society's Challenges and Demands, Two Volume Set*, pages 329–334. CRC Press.

Hoek, E. (2000). *Practical Rock Engineering*. Rocscience, Toronto, 2000 ed. edition.

Huang, S., Lv, Y., Peng, Y., Zhang, L., and Xiu, L. (2015). Effect of Different Groundwater Levels on Seismic Dynamic Response and Failure Mode of Sandy Slope. *PLoS One*, 10(11).

Hudson, J. and Harrison, J. (2000). *Engineering Rock Mechanics*. Elsevier Science Ltd., Oxford, UK.

Hungr, O., Leroueil, S., and Picarelli, L. (2013). The Varnes classification of landslide types, an update. *Landslides*, 11(2):167–194.

ISRM (1978). Suggested Methods for Determining Tensile Strength of Rock Materials. In *The Complete ISRM Suggested Methods for Rock Characterization, Testing and Monitoring:1974-2006*, pages 99–103. ISRM & ISRM Turkish National Group.

ISRM (2007a). Part 1. Suggested Methods for Determining the Uniaxial Compressive Strength of Rock Materials. In *The Complete ISRM Suggested Methods for Rock Characterization, Testing and Monitoring:1974-2006*, pages 137–138. ISRM & ISRM Turkish National Group.

ISRM (2007b). Part 2. Suggested Method for determinng deformability of rock

materials in uniaxial compression. In *The Complete ISRM Suggested Methods for Rock Characterization, Testing and Monitoring:1974-2006*, pages 138–140.

Jaboyedoff, M., Leibundgut, G., Penna, I., Dahal, R. K., Sevkota, S., and Sudmeier, K. (2015). Characterization of the Jure (Sindhupalchok, Nepal) Landslide by TLS and field investigations. volume 17 of *EGU2015-11858-1*. Geophysical Research Abstracts.

Kargel, J. S., Leonard, G. J., Shugar, D. H., Haritashya, U. K., Bevington, A., Fielding, E. J., Fujita, K., Geertsema, M., Miles, E. S., Steiner, J., Anderson, E., Bajracharya, S., Bawden, G. W., Breashears, D. F., Byers, A., Collins, B., Dhital, M. R., Donnellan, A., Evans, T. L., Geai, M. L., Glasscoe, M. T., Green, D., Gurung, D. R., Heijenk, R., Hilborn, A., Hudnut, K., Huyck, C., Immerzeel, W. W., Liming, J., Jibson, R., Kääb, A., Khanal, N. R., Kirschbaum, D., Kraaijenbrink, P. D. A., Lamsal, D., Shiyin, L., Mingyang, L., McKinney, D., Nahirnick, N. K., Zhuotong, N., Ojha, S., Olsenholler, J., Painter, T. H., Pleasants, M., Pratima, K. C., Yuan, Q. I., Raup, B. H., Regmi, D., Rounce, D. R., Sakai, A., Donghui, S., Shea, J. M., Shrestha, A. B., Shukla, A., Stumm, D., Kooij, M. v. d., Voss, K., Xin, W., Weihs, B., Wolfe, D., Lizong, W., Xiaojun, Y., Yoder, M. R., and Young, N. (2016). Geomorphic and geologic controls of geohazards induced by Nepal's 2015 Gorkha earthquake. *Science*, 351(6269):aac8353.

KathmanduPost (2014). Landslip Dams Sunkoshi River.

Kattelmann, R. (1991). Hydrologic regime of the Sapt Kosi basin, Nepal. In *Hydrology for Water Management of Large River Basins*, pages 139–148.

Laouafa, F. and Darve, F. (2002). Modelling of Slope Failure by a Material Instability Mechanism. *Computers and Geotechnics*, 29(4):301–325.

Lillesø, J., Shrestha, T., Dhakal, L., Nayaju, R., and Shrestha, R. (2005). The Map of Potential vegetation in Nepal. A Forestry/Agroecological/Biodiversity classification system. *Forest & Landscape Denmark*.

Lu, Y. (2015). Deformation and failure mechanism of slope in three dimensions. *Journal of Rock Mechanics and Geotechnical Engineering*, 7(2):109–119.

MoI (2014). Report on Jure Landslide, Mankha VDC, Sindhupalchowk District. Technical report, Nepal Government.

Mugnier, J. L., Gajurel, A., Huyghe, P., Jayangondaperumal, R., Jouanne, F., and Upreti, B. (2013). Structural interpretation of the great earthquakes of the last millennium in the central Himalaya. *Earth-Science Reviews*, 127:30–47.

Nilsen, B. and Palmstrøm, A. (2000). *Engineering Geology and Rock Engineering*. Handbook No. 2. Norwegian Group of Rock Mechanics.

NPC (2015). Nepal Earthquake 2015, Post Disaster Needs Assessment, Volume A: Key Findings. Technical report, Government of Nepal National Planning Commission, Kathmandu.

NSET (2015). Gorkha Earthquake | Situation of Earthquake | NSET-Nepal, Earthquake Safe Communities in Nepal by 2020.

Panthi, K. K. (2006). *Analysis of Engineering Geological Uncertainties Related to Tunnelling in Himalayan Rock Mass Conditions*. Fakultet for ingeniørvitenskap og teknologi.

Panthi, K. K. (2016). Discussions regarding this Master's Thesis "Earthquake and Monsoon Induced Slope Failure Effects on Hydropower Projects : An Analysis along the Sunkoshi Valley, Nepal".

Parameswaran, R. M., Natarajan, T., Rajendran, K., Rajendran, C. P., Mallick, R., Wood, M., and Lekhak, H. C. (2015). Seismotectonics of the April–May 2015 Nepal earthquakes: An assessment based on the aftershock patterns, surface effects and deformational characteristics. *Journal of Asian Earth Sciences*, 111:161–174.

Parker, R. N., Densmore, A. L., Rosser, N. J., de Michele, M., Li, Y., Huang, R., Whadcoat, S., and Petley, D. N. (2011). Mass wasting triggered by the 2008 Wenchuan earthquake is greater than orogenic growth. *Nature Geosci*, 4(7):449–452.

Pokharel, J. R., Regmi, S. B., Bhattarai, D. R., Devkota, L. B., Adhikari, T. L., Rajauria, A., Subedi, M., and Dawadi, M. (2014). A Report on Study of Sunkoshi Landslide Dam in Jure, Sindhupalchowk. Technical report, Nepal Engineers' Association, Pulchowk, Lalitpur, Nepal.

Rajendran, C. P. and Rajendran, K. (2005). The status of central seismic gap: a perspective based on the spatial and temporal aspects of the large Himalayan earthquakes. *Tectonophysics*, 395(1–2):19–39.

Rocscience (2016a). DIPS - Graphical and Statistical Analysis of Orientation Data.

Rocscience (2016b). Phase² - Finite Element Analysis for Excavation and Slopes.

Sandøy, G. (2012). *Back-analysis of the 1756 Tjellefonna rockslide, Langfjorden*. Masters Thesis, Norwegian University of Science and Technology, Department of Geology and Mineral Resources Engineering.

Sato, H. P. and Harp, E. L. (2009). Interpretation of earthquake-induced landslides triggered by the 12 May 2008, M7.9 Wenchuan earthquake in the Beichuan area, Sichuan Province, China using satellite imagery and Google Earth. *Landslides*, 6(2):153–159.

Shah, A. A. (2013). Earthquake geology of Kashmir Basin and its implications for future large earthquakes. *Int J Earth Sci (Geol Rundsch)*, 102(7):1957–1966.

Shrestha, P. K. and Panthi, K. K. (2013). Analysis of the plastic deformation behavior of schist and schistose mica gneiss at Khimti headrace tunnel, Nepal. *Bull Eng Geol Environ*, 73(3):759–773.

Stead, D. and Eberhardt, E. (2013). Understanding the mechanics of large landslides. 6, Padua, Italy. Sapienza Università Editrice.

Stead, D., Eberhardt, E., and Coggan, J. S. (2006). Developments in the characterization of complex rock slope deformation and failure using numerical modelling techniques. *Engineering Geology*, 83(1–3):217–235.

USGS (2015a). Magnitude 7.8 Earthquake in Nepal & Aftershocks | Science Features.

USGS (2015b). USGS M7.8 - 36km E of Khudi, Nepal. http://earthquake.usgs.gov/earthquakes/eventpage/us20002926#general Accessed on 4/26/2016, 1:32:54 PM.

Webb, A. A. G., Schmitt, A. K., He, D., and Weigand, E. L. (2011). Structural and geochronological evidence for the leading edge of the Greater Himalayan Crystalline complex in the central Nepal Himalaya. *Earth and Planetary Science Letters*, 304(3–4):483–495.

Wu, J.-H., Wang, W.-N., Chang, C.-S., and Wang, C.-L. (2005). Effects of Strength Properties of Discontinuities on the Unstable Lower Slope in the Chiu-fen-erh-shan Landslide, Taiwan. *Engineering Geology*, 78(3–4):173–186.

Wyllie, D. C. and Mah, C. (2004). *Rock Slope Engineering*. CRC Press.

Yamada, M., Wang, G., and Mukai, K. (2013). The Classification and Features of Earthquake-Induced Landslides in the World. In Ugai, K., Yagi, H., and Wakai, A., editors, *Earthquake-Induced Landslides*, pages 117–124. Springer Berlin Heidelberg. DOI: 10.1007/978-3-642-32238-9_13.

APPENDICES

Appendix A: Laboratory Results

1. Tilt Test

Sample	Direction	Basic Friction Angle, degrees								Average, degrees		
1	A1-A2	22.0	24.7	22.0	23.4	23.1	25.8	26.4	25.2	24.1	24.8	**24.7**
	A2-A1	24.4	26.5	24.9	27.0	22.4	26.0	25.9	26.9	25.5		
	B1-B2	25.6	24.9	24.3	24.4	23.4	23.2	26.7	24.8	24.7		
	B2-B1	22.1	26.1	24.7	25.8	24.3	24.6	27.2	23.4	24.8		
2	A1-A2	22.0	24.2	23.2	26.5	22.1	26.3	25.0	23.4	24.1	24.2	
	A2-A1	25.2	23.8	26.8	23.7	24.2	26.0	23.0	24.4	24.6		
	B1-B2	23.1	23.6	25.3	24.2	25.1	23.8	22.6	24.9	24.1		
	B2-B1	26.0	24.8	23.6	21.4	22.5	25.5	25.0	23.4	24.0		
3	A1-A2	26.5	27.3	24.2	24.0	26.2	25.8	25.9	25.3	25.7	25.0	
	A2-A1	26.8	27.2	25.5	26.1	24.9	25.9	23.0	24.6	25.5		
	B1-B2	20.9	23.8	25.8	25.8	23.9	23.4	23.0	25.4	24.0		
	B2-B1	23.6	25.6	25.7	24.7	24.6	24.9	24.9	25.6	25.0		

2. Uniaxial Compression Test

Sample No.	UCS (MPa)	E-modulus (GPa)	Poissons Ratio
1	89	34.06	0.47
2	81.6	31.69	0.57
3	88.8	34.06	0.4
4	87	33.32	0.54
5	78.1	30.05	0.37
Average	**84.9**	**32.636**	**0.47**

3. Brazil Test

Sample	Thickness (t), mm	Diameter (D), mm	Load at failure (P), KN	Tensile strength (σ_t), Mpa
1	25.34	49.80	21.51	10.84
2	25.31	49.54	18.85	9.56
3	25.36	49.80	18.35	9.24
4	25.76	49.90	17.36	8.59
5	25.52	49.75	19.64	9.84
6	25.09	49.69	16.52	8.43
Average				**9.42**

$$\sigma_t = \frac{0.636 * P}{D_t}$$

Appendix B: Official Letters

NTNU
Norwegian University of
Science and Technology

Faculty of Engineering Science and Technology
Department of Geology and
Mineral Resources Engineering

Ref: no. N-2

Date: 05.08.2015

The Generation Directorate
Nepal Electricity Authority
Ratnapark, Kathmandu

Subject: Data Collection for MSc Thesis Work

This is to certify that Mr. Nabin Basnet, a Nepalese citizen and MSc fellow at the Department of Geology and Mineral Resources Engineering - Norwegian University of Science and Technology (NTNU), is writing MSc research thesis in rock engineering". His MSc thesis will focus on the earthquake impact in the infrastructures with particular focus on slope stability and foundation stability issues for roads and hydropower projects.

Mr. Basnet is visiting to Nepal during this summer to collect necessary information and date for his research topic. Hence, I kindly request The Generation Directorate of Nepal Electricity Authority (NEA) to help him by giving access to the information and data associated to the damage occurred in the Hydropower Plants due to Earthquake event of this year and the design related information.

Your help will be a contribution in building highly skilled capabilities, which is a real need to Nepal and will be highly appreciated.

Sincerely yours,

Krishna Panthi

Dr. Krishna Kanta Panthi
Associate Professor of Rock Engineering

NTNU
Norges teknisk-naturvitenskapelige universitet
Institutt for geologi og bergteknikk
7491 Trondheim

Postal Address:
Semsælands Vei 1
7491, Trondheim, Norway

email:
krishna.panthi@ntnu.no
www.ntnu.no

Telephone:
+4773594824 (direct)
+4773594800
Fax: +47 73594814

Dr. Krishna Kanta Panthi
Associate Professor

NTNU
Norwegian University of
Science and Technology

Faculty of Engineering Science and Technology
Department of Geology and
Mineral Resources Engineering

Ref: no. N-3

Date: 19.08.2015

The Department of Mines and Geology
Lazimpat, Kathmandu

Subject: Lab Testing Rock Samples for MSc Thesis Research

This is to certify that Mr. Nabin Basnet, a Nepalese citizen and MSc fellow at the Department of Geology and Mineral Resources Engineering - Norwegian University of Science and Technology (NTNU), is writing MSc research thesis in rock engineering". His MSc thesis will focus on the earthquake impact in the infrastructures with particular focus on slope stability and foundation stability issues for roads and hydropower projects.

Mr. Basnet has collected some rock samples during this summer to carry out rock mechanical testing at the Stats-of-art engineering geological laboratory of the Department of Geology and Mineral Resources Engineering of NTNU. Hence, I kindly request The Department of Mines and Geology giving approval to bring selected rock samples to this University located in Trondheim, Norway.

Your help will be a contribution in building highly skilled capabilities, which is a real need to Nepal and will be highly appreciated.

Sincerely yours,

Krishna Panthi

Dr. Krishna Kanta Panthi
Associate Professor of Rock Engineering

NTNU
Norwegian University of Science and Technology
Dep. of Geology and Mineral Resources Engineering
NO-7491 Trondheim

Postal Address:	email:	Telephone:	Dr. Krishna Kanta Panthi
Semsælands Vei 1	krishna.panthi@ntnu.no	+4773594824 (direct)	Associate Professor
7491, Trondheim, Norway	www.ntnu.no	+4773594800	
		Fax: +47 73594814	